Mon. Not. R. Astron. Soc. **339,** 335–352 (2003)

Gravitational microlensing of γ-ray blazars

Diego F. Torres,[1,2]★ Gustavo E. Romero,[3] Ernesto F. Eiroa,[4]
Joachim Wambsganss[5] and Martín E. Pessah[6]

[1]*Lawrence Livermore National Laboratory, 7000 East Ave, L-413, Livermore, CA 94550, USA*
[2]*Physics Department, Princeton University, NJ 08544, USA*
[3]*Instituto Argentino de Radioastronomía (IAR), CC 5, 1894 Villa Elisa, Buenos Aires, Argentina*
[4]*Instituto de Astronomía y Física del Espacio, CC 67, Suc. 28, 1428, Buenos Aires, Argentina*
[5]*Universität Potsdam, Institut für Physik, Am Neuen Palais 10, 14469 Potsdam, Germany*
[6]*Steward Observatory, University of Arizona, AZ 85721, USA*

Accepted 2002 October 18. Received 2002 September 30; in original form 2002 May 23

ABSTRACT

We present a detailed study of the effects of gravitational microlensing on compact and distant γ-ray blazars. These objects have γ-ray-emitting regions that are small enough to be affected by microlensing effects produced by stars lying in intermediate galaxies. We compute the gravitational magnification taking into account effects of the lensing and show that, whereas the innermost γ-ray spheres can be significantly magnified, there is little magnification either for very high γ-ray energies or for lower (radio) frequencies (because these wavelengths are emitted from larger regions). We analyse the temporal evolution of the gamma-ray magnification for sources moving in a caustic pattern field, where the combined effects of thousands of stars are taken into account using a numerical technique. We propose that some of the unidentified γ-ray sources (particularly some of those lying at high galactic latitude with gamma-ray statistical properties that are very similar to detected γ-ray blazars) are indeed the result of gravitational lensing magnification of background undetected active galactic nuclei (AGN). This is partly supported from a statistical point of view: we show herein as well, using the latest information from the third EGRET catalogue, that high-latitude γ-ray sources have similar averaged properties to already detected γ-ray AGN. Some differences between both samples, regarding the mean flux level, could also be understood within the lensing model. With an adequate selection of lensing parameters, it is possible to explain a variety of γ-ray light curves with different time-scales, including non-variable sources. The absence of strong radio counterparts could be naturally explained by differential magnification in the extended source formalism.

Key words: gravitational lensing – galaxies: active – gamma-rays: observations – gamma-rays: theory.

1 INTRODUCTION

The first extragalactic γ-ray source detected was the quasar 3C 273, which was observed by the *COS-B* satellite in a particularly active state in the 1970s (Swanenburg et al. 1978). Since then, many active galactic nuclei (AGN) have been detected at high energies, most of them belonging to the blazar class (e.g. Mukherjee 2001). The third EGRET catalogue of point-like sources currently lists 66 detections labelled as AGN (Hartman et al. 1999). Notwithstanding, a large number of γ-ray sources, scattered along the entire sky, remain unidentified at present.

★E-mail: dtorres@igpp.ucllnl.org

The unidentified γ-ray sources at low latitudes are probably related to several distinct galactic populations (Romero 2001). Among them there might be pulsars (e.g. Kaspi et al. 2000; Zhang, Zhang & Cheng 2000; Camilo et al. 2001; D'Amico et al. 2001; Torres, Butt & Camilo 2001d), supernova remnants in interaction with molecular clouds (Combi & Romero 1995; Esposito et al. 1996; Sturner, Dermer & Mattox 1996; Combi, Romero & Benaglia 1998; Butt et al. 2001; Combi et al. 2001; Torres et al. 2002b), stellar-size black holes (Punsly 1998a,b; Punsly et al. 2000), X-ray transients (Romero et al. 2001), persistent microquasars (Paredes et al. 2000; Kaufman Bernadó, Romero & Mirabel 2002), and massive stars with strong stellar winds (Benaglia et al. 2001). Some of these kinds of stellar objects present statistical positional correlation with unidentified

EGRET sources [far from what is expected as a random result, e.g. Romero, Benaglia & Torres (1999); Torres et al. (2001b)]. Pulsars, however, remain as the only confirmed low-latitude population, since pulsed γ-ray radiation has already been detected for at least six different sources (Thompson et al. 1999; Kaspi et al. 2000; Thompson 2001), five of them included in the third EGRET catalogue (Hartman et al. 1999).

Gehrels et al. (2000) have shown that the mid-latitude sources are different from the bright population of unidentified sources along the Galactic plane. Some of the detections ($5^\circ < |b| < 30^\circ$) are thought to be associated with the Gould Belt (Grenier 2000; Gehrels et al. 2000), a starburst region lying at $\sim$600 pc from Earth. Few other sources, at higher latitudes, could be the result of electrons being accelerated at the shock waves of forming clusters of galaxies (Totani & Kitayama 2000). However, for many of the high-latitude sources, no explanation seems to be available other than they are AGN as yet undetected at lower energies. This is particularly clear when one looks at the variability levels of the associated light curves: models requiring a large acceleration region, such as clusters of galaxies, would produce non-variable sources, contrary to what is found for most of the high-latitude sources.

All identified 66 EGRET AGN are also strong radio sources with flat spectra, as expected from synchrotron jet-like sources where the γ-ray flux is the result of inverse Compton scattering (Mattox et al. 1997). However, no strong radio source appears within the contours of the unidentified high-latitude EGRET sources. In this paper, we shall develop a model, briefly outlined by Torres, Romero & Eiroa (2002a), which focuses precisely on that difference and provides an explanation as to why some of the high-latitude unidentified sources might not be detected at low frequencies. The main feature of such a model is that it will account for the γ-ray properties of the high-latitude gamma-ray detections resorting to differential gravitational lensing magnification of background, high-redshift, AGN with otherwise undetected γ-ray emission. Since these objects have different sizes at different wavelengths, differential microlensing effects will lead to a magnification of the innermost γ-ray-emitting regions, whereas the radio emission will be largely unmagnified, therefore remaining under the detection threshold. Other wavelengths, depending on their emission size will be magnified too. Optical emission, for example, could well be cospatial with the innermost γ-spheres, and thus be subject to similar phenomena.

The gravitational light deflection effect by compact objects on background sources is commonly called microlensing (e.g. Paczyński 1986). A source would be affected by different magnifications, depending on its position. Typically, source, lens and observer move relative to each other, and therefore, this translates into a variable flux measured for the background source. Observationally, there are two interesting regimes of microlensing. Local microlensing deals with the light deflection effects by stars inside the Milky Way disc on stars in the Galactic bulge. Here the probability for a microlensing event is of the order of $\times 10^{-6}$. This means that it is necessary to monitor millions of stars in order to see a few occurrences. However, despite this small probability, various teams have been very successful in detecting this kind of event in recent years (for a review see Paczyński 1996). The other interesting regime of microlensing is usually called quasar microlensing, but it can be applied to any other compact source at moderate to high redshift. In this case, an intervening galaxy provides the surface mass density in stars (or other compact objects) which act as microlenses on the background quasar (for a review see Wambsganss 2001). Recently, this kind of microlensing has been suggested for other astrophysical sources as well, e.g. gamma-ray bursts (Williams & Wijers 1997), gamma-ray burst afterglows (Garnavich, Loeb & Stanek 2000; Koopmans & Wambsganss 2001; Mao & Loeb 2001), and superluminal shocks in extragalactic radio sources (Romero, Surpi & Vucetich 1995; Koopmans & de Bruyn 2000). The gamma-ray sources discussed here are another type of astrophysical object for which microlensing possibly plays an important role.

We recall that gravitational light deflection is basically an achromatic phenomenon, being a geometric effect predicted by general relativity, i.e. the deflection angle does not depend on the energy of the photon. However, it is nevertheless possible to have chromaticity effects when the size of the source changes with the observing wavelength. A large source is typically less affected by a microlensing magnification than a small source (Wambsganss & Paczyński 1991). This size-induced chromaticity will be an essential ingredient of our model.

2 UNIDENTIFIED γ-RAY SOURCES AT HIGH LATITUDES

2.1 Sample and photon spectral index

Previous population studies using the second EGRET catalogue have already remarked that part of the sample of high-latitude unidentified sources is consistent with an isotropic population, a fact that supports an extragalactic origin for these detections (Özel & Thompson 1996). In what follows, we shall make a comparison between the properties of identified γ-ray AGN in the third EGRET catalogue and high-latitude unidentified sources. We shall choose the lower cut-off in latitude as $|b| = 30^\circ$, in order to avoid possible contamination from Gould Belt sources. There are 45 3EG unidentified sources within this latitude range; we provide details on these sources in Table 1.

Fig. 1 shows the distribution of the γ-ray photon spectral index for both sets of sources, 45 unidentified EGRET sources and 66 detected EGRET AGN. The mean value of the photon index is 2.36 ± 0.36 for AGN and 2.49 ± 0.34 for the unidentified detections. They are compatible within the uncertainties and, on average, steeper than what is observed for low-latitude sources, which are thought to belong to our own Galaxy.

2.2 Variability

Several models for γ-ray sources in our Galaxy predict non-variable emission during the time-scale of EGRET observations. AGN, in contrast, are expected to present a variable flux emission. Variability is, in the case where we were able to quantify it with some degree of precision, a powerful tool to probe the nature of the sources. Visual inspection of the flux evolution through the different viewing periods is obviously a first indication of the variability status of any given source. However, fluxes are usually the result of only a handful of incoming photons, experimental errors are sometimes huge and their origin uncertain, and consequently more reliable ways of quantizing the flux evolution should be devised: these are known as variability indices. Two such indices have been recently introduced in the literature and applied to 3EG sources so far (Tompkins 1999, index τ; Torres et al. 2001a, index I). In general, statistical results from these two indices are well correlated (see Torres, Pessah & Romero 2001c for a discussion). Here we shall adopt the index I, previously used in blazar variability analysis (Romero, Combi & Colomb 1994) and applied to some of the 3EG sources

Table 1. The 45 unidentified sources considered in the analysis. We list their 3EG catalogue name, their Galactic coordinates, spectral index, variability index, and the values of $\langle F\rangle$ used to define I in equation (2). We also provide the 3EG P1234 fluxes, F. $\langle F\rangle$ and F are in units of 10^{-8} photon cm^{-2} s^{-1}. The columns labelled τ, $\tau_{\rm min}$ and $\tau_{\rm max}$, give the central value of Tompkins (1999) index for variability and their 68 per cent CL lower and upper limit deviations, respectively. The pulsar population has $\langle\tau\rangle < 0.1$, whereas typical AGN have $\langle\tau\rangle \sim 0.7$. Extreme upper limits for τ, the maximum of which is 10 000, imply possibly strong variability.

3EG JSource	l	b	Spectral index	I	τ	$\tau_{\rm min}$	$\tau_{\rm max}$	$\langle F\rangle$	F
0245+1758	157.62	−37.11	2.61	2.74	2.63	0.73	2287	11.3	8.8
0404+0700	184.00	−32.15	2.65	1.50	0.34	0.00	1.65	13.5	11.1
0512−6150	271.25	−35.28	2.40	2.34	0.00	0.00	0.55	10.8	7.2
0530−3626	240.94	−31.29	2.63	1.62	17.8	15.8	0.61	0.15	2.28
0808+4844	170.46	32.48	2.15	0.90	0.00	0.00	0.39	12.2	10.7
0808+5114	167.51	32.66	2.76	1.53	0.00	0.00	0.73	13.5	8.7
0910+6556	148.30	38.56	2.20	1.79	0.49	0.00	1.14	9.2	5.9
1457−1903	339.88	34.60	2.67	2.72	0.42	0.00	3.64	13.9	8.1
1504−1537	344.04	36.38	–	2.73	10.33	1.21	9999.0	12.9	8.8
1600−0351	6.30	34.81	2.65	7.26	68.17	0.00	9999.0	9.7	9.9
1621+8203	115.53	31.77	2.29	0.34	0.00	0.00	0.29	11.5	7.4
1733+6017	89.12	32.94	3.00	1.82	0.39	0.00	1.38	16.9	8.7
1958−4443	354.85	−30.13	–	7.43	58.02	5.85	9999.0	11.3	6.4
2034−3110	12.25	−34.64	3.43	5.26	2.88	0.89	155.0	6.8	5.2
2219−7941	310.64	−35.06	2.50	1.37	0.00	0.00	0.51	19.8	13.5
2243+1509	82.69	−37.49	–	11.11	3.42	0.88	3097	7.4	9.9
2248+1745	86.00	−36.17	2.11	2.20	1.07	0.43	3.98	20.2	12.9
2255+1943	89.03	−35.43	2.36	5.54	2.31	0.80	48.6	14.2	5.8
0038−0949	112.69	−72.44	2.70	2.71	0.00	0.00	0.89	15.3	12.0
0118+0248	136.23	−59.36	2.63	2.28	5.17	0.90	9999.0	11.5	5.1
0130−1758	169.71	−77.11	2.50	0.10	0.00	0.00	0.38	13.5	11.6
0159−3603	248.89	−73.04	2.89	1.26	0.00	0.00	1.16	11.9	9.8
0215+1123	153.75	−46.37	2.03	3.67	10.06	1.19	9999.0	8.0	9.3
0253−0345	179.70	−52.56	–	7.99	16.44	1.38	9999.0	5.0	6.2
0348−5708	269.35	−46.79	–	4.76	6.60	1.29	9999.0	5.8	3.8
0917+4427	176.11	44.19	2.19	1.69	0.00	0.00	0.34	18.6	13.8
1009+4855	166.87	51.99	1.90	1.14	0.00	0.00	0.60	7.7	4.8
1052+5718	149.47	53.27	2.51	2.02	0.21	0.00	0.74	6.8	5.0
1133+0033	264.52	57.48	2.73	4.44	0.71	0.16	2.00	9.1	3.7
1134−1530	277.04	43.48	2.70	3.35	2.85	1.11	51.5	17.2	9.9
1212+2304	235.57	80.32	2.76	5.65	78.82	0.00	9999.0	6.3	3.3
1219−1520	291.56	46.82	2.52	3.16	1.78	0.74	13.7	8.9	4.1
1222+2315	241.87	82.39	–	1.95	61.09	2.44	9999.0	6.9	5.7
1227+4302	138.63	73.33	–	3.20	61.09	2.44	9999.0	6.7	4.6
1234−1318	296.43	49.34	2.09	2.03	0.42	0.12	0.81	11.0	7.3
1235+0233	293.28	65.13	2.39	1.04	0.23	0.00	0.65	10.5	6.8
1236+0457	292.59	67.52	2.48	1.70	0.00	0.00	1.45	7.3	6.5
1310−0517	311.69	57.25	2.34	1.28	2.94	1.69	7.92	11.4	7.9
1323+2200	359.33	81.15	1.86	5.17	2.69	0.93	46.8	10.1	5.2
1337+5029	105.40	65.04	1.83	2.85	0.54	0.00	1.35	10.0	9.2
1347+2932	47.31	77.50	2.51	1.10	0.48	0.00	1.45	15.3	9.6
1424+3734	66.82	67.76	3.25	1.90	0.01	0.00	9999.0	18.0	–
2241−6736	319.81	−45.02	2.39	1.25	0.00	0.00	1.09	16.6	–
2251−1341	52.48	−58.91	2.43	5.17	9.49	1.58	9999.0	9.7	6.5
2255−5012	338.75	−58.12	2.79	1.59	0.41	0.00	1.46	12.7	9.2

by Zhang et al. (2000) and Torres et al. (2001a,c) as our main quantitative evaluation of variability, although the results for τ are also given in Table 1. The basic idea behind the index I is to directly compare the flux variation of any given source with that shown by known γ-ray pulsars, which are assumed to be an intrinsically non-variable population. This index, in contrast to Tompkins' index τ (Tompkins 1999), uses only the publicly available data of the 3EG catalogue.

Let us recall the basic elements that are used to define the I index. First, a mean weighted value for the EGRET flux is computed:

$$\langle F\rangle = \left[\sum_{i=1}^{N_{\rm vp}} \frac{F(i)}{\epsilon(i)^2}\right] \times \left[\sum_{i=1}^{N_{\rm vp}} \frac{1}{\epsilon(i)^2}\right]^{-1}, \quad (1)$$

where $N_{\rm vp}$ is the number of single viewing periods, $F(i)$ is the observed flux in the ith period and $\epsilon(i)$ is the corresponding error. For those observations in which the significance ($\sqrt{TS}$ in the EGRET catalogue) is greater than 2σ, the error is $\epsilon(i) = F(i)/\sqrt{TS}$. For those observations that are, in fact, upper bounds on the flux, it is assumed that both $F(i)$ and $\epsilon(i)$ are half the value of the upper bound.

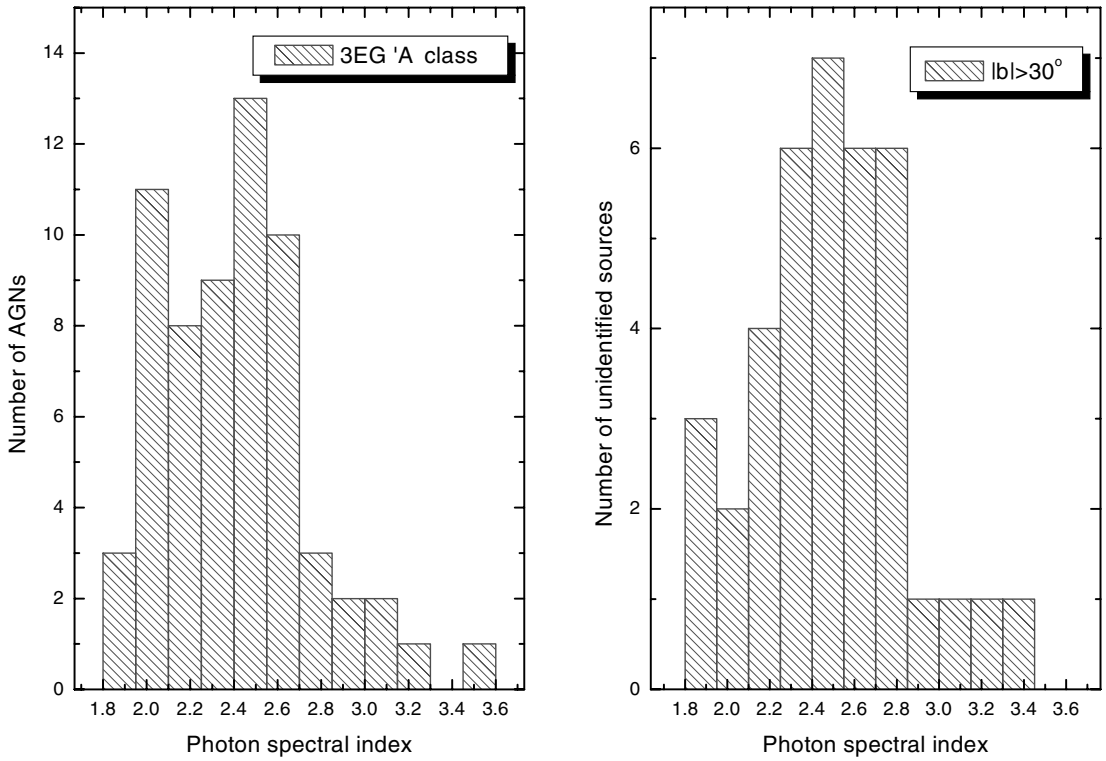

Figure 1. Photon spectral index comparison. The left-hand panel shows the distribution for the 66 detected AGN, dubbed A, in the third EGRET catalogue. The right-hand panel shows the corresponding distribution for the $|b| > 30^\circ$ unidentified sources. This figure can be seen in colour in the online version of the journal on *Synergy*.

The fluctuation index μ is defined as

$$\mu = 100\sigma_{\rm sd}\langle F\rangle^{-1}. \quad (2)$$

In this expression, $\sigma_{\rm sd}$ is the standard deviation of the flux measurements. This fluctuation index is also computed for the confirmed γ-ray pulsars in the 3EG catalogue, assuming the physical criterion that pulsars are non-variable γ-ray sources. The averaged statistical index of variability, I, is then given by the ratio

$$I = \frac{\mu_{\rm source}}{\langle\mu\rangle_{\rm pulsars}}. \quad (3)$$

Once the index is defined, we need to clarify the thresholds for variability. Following Torres et al. (2001c), clearly variable sources will be those with $I > 5$, possibly variable sources will have $2.5 < I < 5$, non-variable sources will have $I < 1.7$ and the remaining sources will be considered as dubious cases. These are very conservative cut-offs: $I > 5$ means that we are asking for the value of I to be 8σ above that of pulsars in order to classify a source as variable.

Fig. 2 compares the I-index distribution for the samples under analysis. The mean value for AGN (left-hand panel) is 3.3 ± 2.6. A possible peak in the plot is seen at $I = 2.5$, which represents a value 4σ above that presented by pulsars. Clearly, most of the AGN are probably variable sources. The mean for the unidentified sources (Fig. 2, right-hand panel) is also high: 3.0 ± 2.3.

Fig. 3 (left-hand panel) shows the variability index I versus the Galactic latitude. The constraint we are imposing on our sample of unidentified sources (to have $|b| > 30^\circ$) can be clearly noticed in the bottom plot. There is not a clear dependence of the variability index with latitude, neither for AGN nor for unidentified sources. The same happens in the plots of Fig. 3 (right-hand panel), where we show the variability index versus the photon spectral index. An apparent trend of increasing the variability status for the steepest sources, already noticed by Torres et al. (2001a) and Reimer (2001), is shown in this figure. However, this is not conclusive since results for a Spearman rank test are in the range of a few per cent for this to be a random phenomenon. An overall characteristic of Figs 2 and 3 is that both samples look quite similar, with no apparent strong deviation from each other shown in terms of variability or photon spectral index distributions.

2.3 Fluxes and possible radio counterparts

Fig. 4 shows the EGRET averaged flux as a function of the photon spectral index and the variability index, respectively. We note that, although there is no apparent difference in the form of the distribution for both samples under consideration, there is a clear contrast in the flux values: whereas most identified γ-ray AGN have fluxes above 10^{-7} photon cm^{-2} s^{-1}, most of the unidentified sources present lower values. This is consistent with what was presented by Gehrels et al. (2000) for sources at latitudes $|b| > 5^\circ$.

This difference in the flux values is also translated into the log N–log F plots we present in Fig. 5. It can be seen there that the linear fits differ significantly. AGN present a fit close to what is expected for an isotropic and uniform population ($F^{-3/2}$), and also similar to what was found using the 2EG catalogue (Özel & Thompson 1996). The unidentified sources, however, present a steeper dependence. The difference in the flux levels is also shown on the x-axis. However, the analysis of the result for the sample of unidentified sources should be performed with extra care, since the errors are far larger, and the number of sources considered is smaller. Additionally, AGN present an apparent lack of sources at $F \sim 30 \times 10^{-8}$ photon cm^{-2} s^{-1}, which should be supported or falsified by future observations.

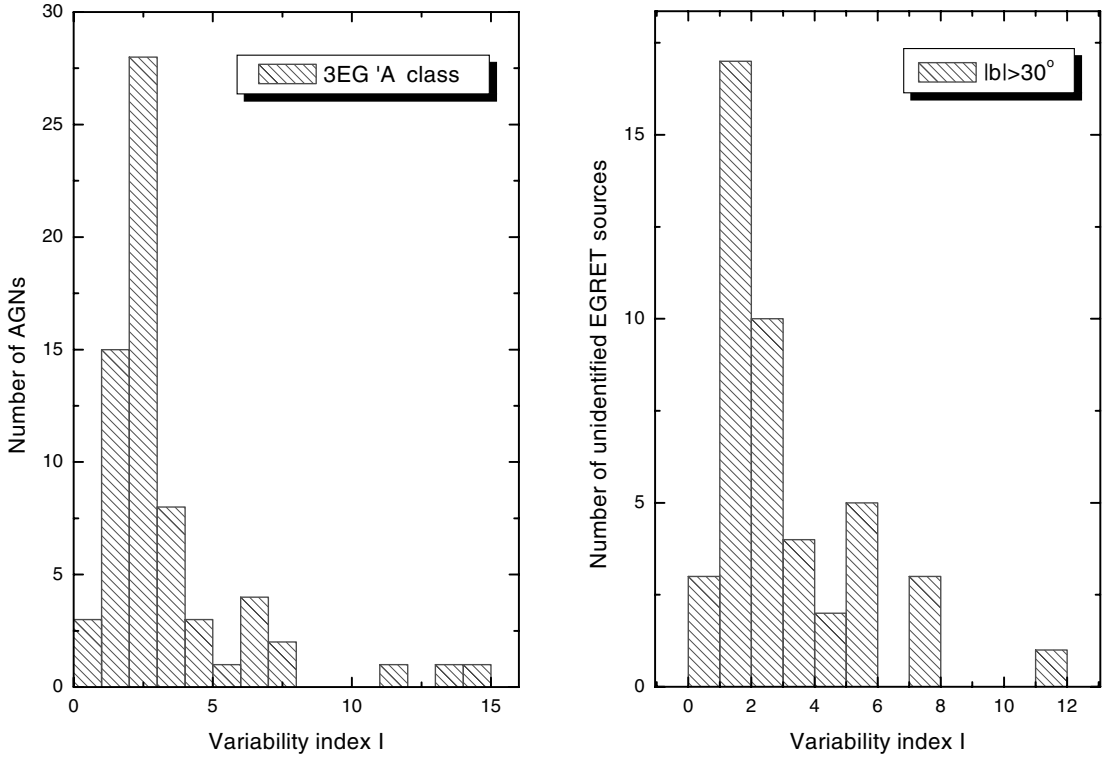

Figure 2. Variability index comparison. The left-hand panel shows the distribution for the 66 detected AGN, dubbed A, in the third EGRET catalogue. The right-hand panel shows the corresponding distribution for the $|b| > 30^\circ$ unidentified sources. This figure can be seen in colour in the online version of the journal on *Synergy*.

Reimer & Thompson (2001) studied in detail the $\log N$–$\log F$ plots obtained from 3EG sources, but also including those sources with a lower confidence level (which did not appear in the published version of the 3EG catalogue). They found that there is a very pronounced contrast between average and peak flux representation in a $\log N$–$\log F$ diagram for the sources above $|b| > 30^\circ$. This is caused by the fact that sources at high latitudes are mostly detected only in some (or in many cases, only in one) viewing periods (see below), when they show their peak flux, leaving the average over the four phases of the experiment in a much lower value. The differences in fluxes between the peak detections of both distributions, although still present, are not so strong as those presented in the P1234 averaged values. As we shall see below, sources showing large fluxes only in one viewing period could be particularly suitable to be explained by microlensing of gamma-ray blazars.

The differences in the $\log N$–$\log F$ plots could be pointing towards one of the following two possibilities.

(i) We are looking at (at least) two different populations; for instance, AGN and a new halo class of high-energy objects.

(ii) These samples are formed mostly by the same kind of objects (AGN), but they present different γ-ray flux levels. This difference could be produced as an extrinsic effect when the sources are further away from us than those that produce the most energetic detections.

If behind both samples there is actually a single class of extragalactic objects, the combined $\log N$–$\log F$ plot should approximately follow an $N \propto F^{-3/2}$ law. The result, given in Fig. 6, confirms this (see also the comments by Reimer & Thompson 2001). This seems to be suggesting that the sample of unidentified sources under consideration is formed by many weak AGN, which at the same time presents a low (i.e. under the thresholds of the corresponding surveys) radio emission. We note that the apparent bump at $F \sim 30 \times 10^{-8}$ photon cm^{-2} s^{-1} continues to appear in the combined plot, since no unidentified sources present such relatively high-γ-ray fluxes.

Recently, Mattox, Hartman & Reimer (2001) have presented a quantitative analysis of potential radio identifications for all 3EG sources. They used radio surveys at 5 GHz, as was done previously for the 2EG catalogue (Mattox et al. 1997), and evaluated an a priori probability for these associations to be physical, based on the positional offsets and radio fluxes of the proposed counterparts. They found that 45 out of the 66 3EG sources classified with 'A' by Hartman et al. (1999) were among the EGRET identifications with the highest probability of being correct. Only one extra possible association in the list of these most likely identifications was not dubbed 'A' in the 3EG catalogue. For each of these 46 associations, they have compiled radio fluxes at 5 GHz, and when available, also those obtained with very-long-baseline interferometry (VLBI). Fig. 7 shows the γ-ray flux of each of these 3EG sources [note that we plot the P1234 EGRET flux of the 3EG source from Hartman et al. (1999), not the flux of the AGN quoted, for instance, in Mattox et al. (1997)] as a function of the radio flux at 5 GHz of the likely counterparts. Most of the detections present a radio flux above 1 Jy, and there is an apparent trend to become more radio loud when the observed γ-ray flux is higher. This is the expected behaviour when the emitted γ-rays have their origin in inverse Compton interactions of the same particle population (leptons) that generate the radio emission, targeting a soft photon field. We have assumed a linear function to the radio-gamma data as is also shown in Fig. 7. There, we indicate with a dashed line, the extension of this linear fit to the

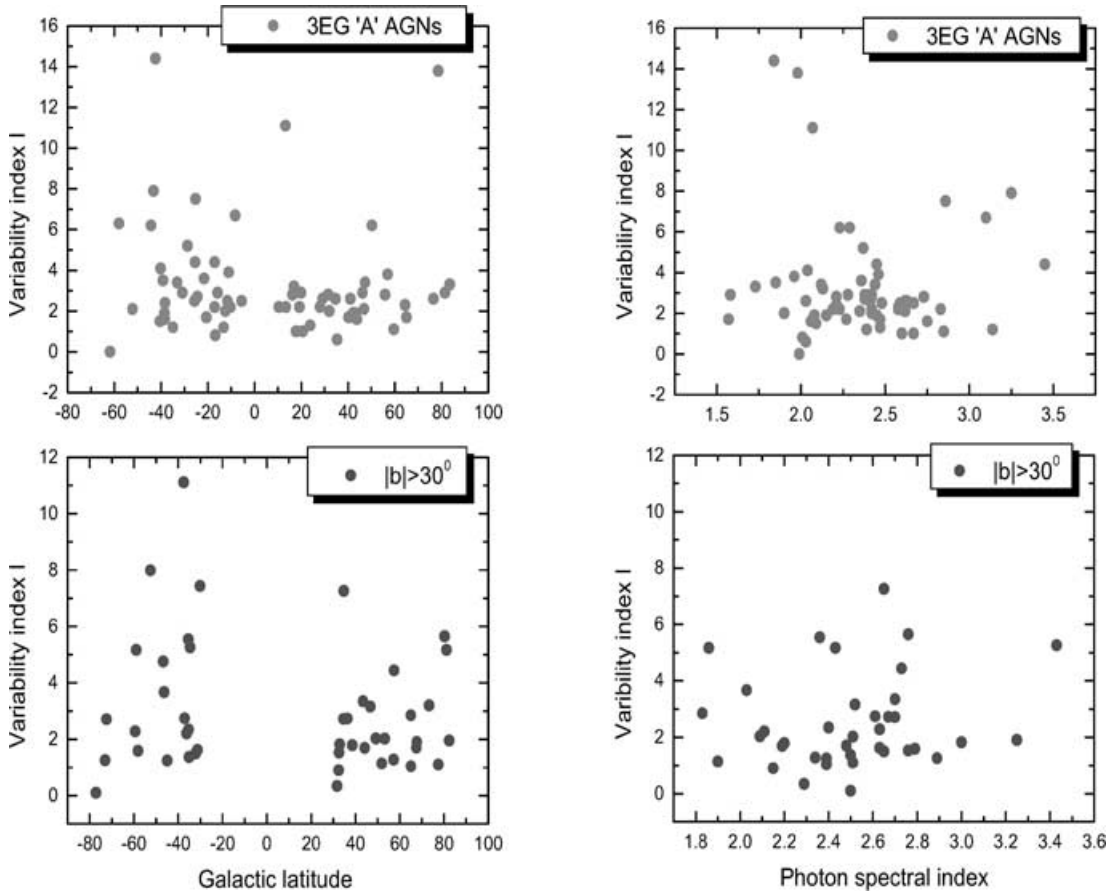

Figure 3. Variability index I (Torres et al. 2001a) versus Galactic latitude (left) and versus photon spectral index (right). This figure can be seen in colour in the online version of the journal on *Synergy*.

region where there are no 3EG 'A' AGN sources. The big vertical box signals the threshold for detectability in the radio surveys used to search for counterparts (∼30 mJy). The middle, lighter coloured box, signals the range of γ-ray fluxes for the unidentified sources considered in this paper. It is apparent, then, that if weak AGN were to approximately follow the linear fit, we could find several γ-ray sources without significant radio flux. Many of them could be those unidentified sources we are studying here. In addition, if γ-ray sources are affected by a differential gravitational lensing effect, this process, as we shall show below, would enhance only the γ-ray emission, keeping the radio fluxes at low levels. This mechanism, then, would be in agreement with what is shown in Fig. 7, provided the associated sources are within the middle box on the left. Of course, this cannot apply to all unidentified sources because, otherwise, it would result in a hole in the source distribution between the already detected AGN and the candidates, at radio flux levels of ∼100 mJy. It should be remembered that sources at high latitude are preferentially identified by their peak flux, which can be much higher than the average. Although population studies are a powerful tool for studying the nature of the unidentified detections, they should be supplemented by a source-by-source analysis.

The main conclusion up to here is that is likely that some of the high-latitude unidentified sources are no more than otherwise undetected AGN, presenting a low or nil (below any current detection threshold) radio flux. General gamma-ray characteristics of both γ-ray blazars and high-latitude unidentified sources are very similar. There remains, however, the question of why, whereas most γ-loud blazars present radio flux at the Jy level, the unidentified sources have no strong radio counterpart at all. If the same mechanism for γ-ray production operates in both groups of objects, why are they so different at lower energies? We shall argue in the next sections that extrinsic effects can result in such a behaviour.

3 γ-RAY BLAZARS AS SOURCES

The fact that some γ-ray blazars have been observed to flare dramatically on time-scales of days imposes severe constraints on the size of the emitting region. The optical depth for intrinsic $\gamma + \gamma \rightarrow e^+ + e^-$ attenuation is (e.g. Schlickeiser 1996)

$$\tau \simeq \sigma_{\rm T} n_\gamma R = \frac{\sigma_{\rm T}}{4\pi c \langle \epsilon \rangle} l, \tag{4}$$

where $\sigma_{\rm T}$ is the Thompson cross-section, n_γ is the γ-ray photon density, $R < ct_{\rm v}$ is the source size inferred from the intrinsic variability time-scale, $\langle \epsilon \rangle$ is the mean photon energy and l is the compactness parameter defined as the ratio of the intrinsic source luminosity to its radius. The optical depth can be written as

$$\tau > 200 \frac{L_{48}}{t_{\rm v}/1\ {\rm d}}, \tag{5}$$

with L_{48} being the luminosity in units of 10^{48} erg s^{-1}. For typical values $t_{\rm v} \sim 1$ d and $L_{48} \sim 1$, the source is opaque, in contrast to the observed fact that γ-ray blazars present a power-law γ-ray spectrum over several decades of energy. This rules out isotropic emission in the rest frame. The emission, consequently, should be beamed.

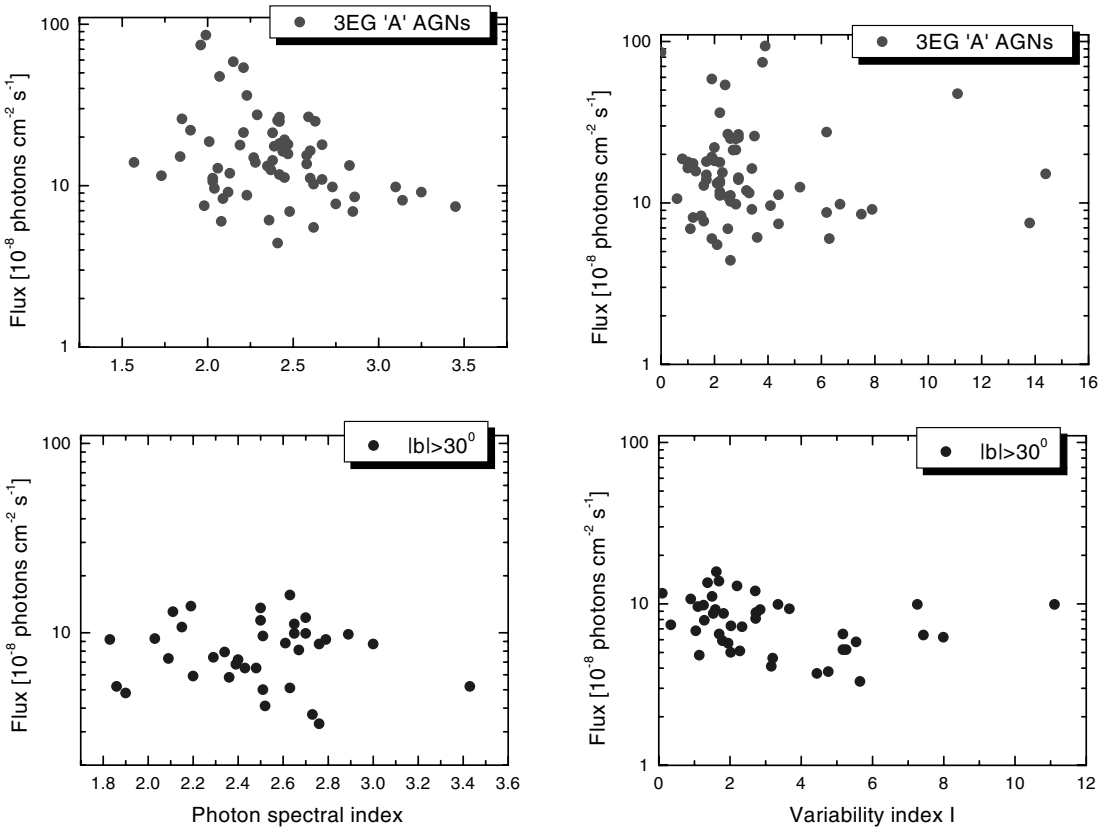

Figure 4. Source fluxes (P1234 Hartman et al. 1999) versus photon spectral index (left) and variability index (right). This figure can be seen in colour in the online version of the journal on *Synergy*.

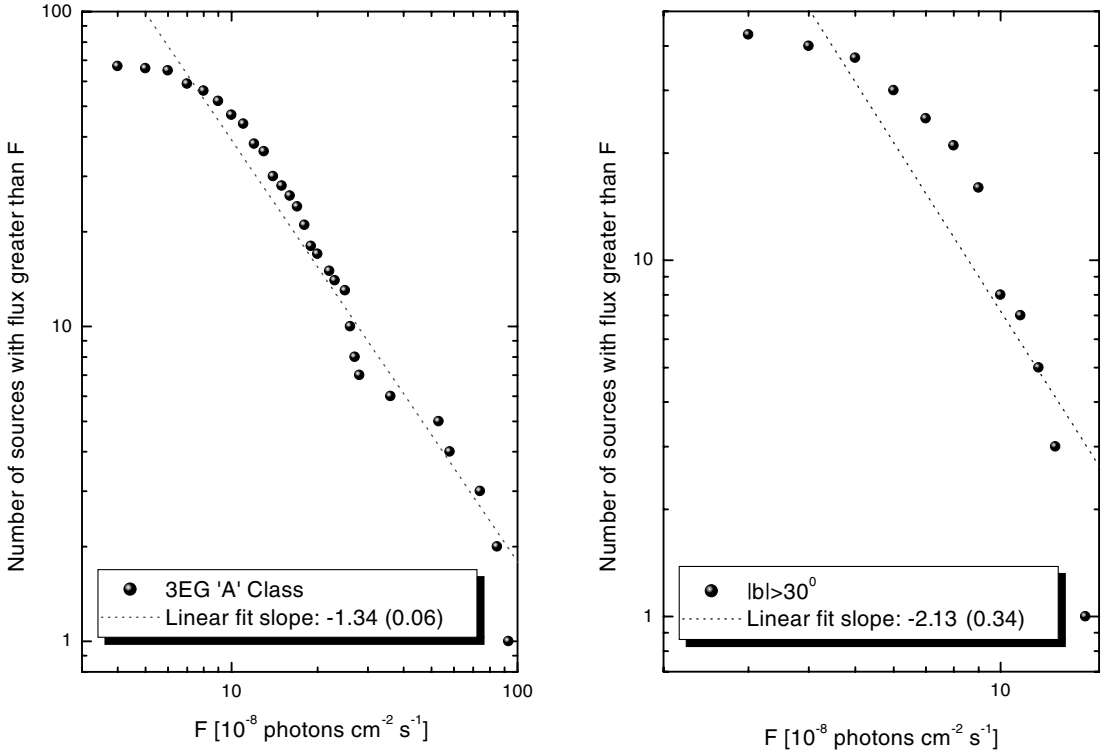

Figure 5. Log *N*–log *F* comparison. The value of the linear fitting slope (and error within parentheses) is shown for each case. *F* is the 3EG P1234 flux. This figure can be seen in colour in the online version of the journal on *Synergy*.

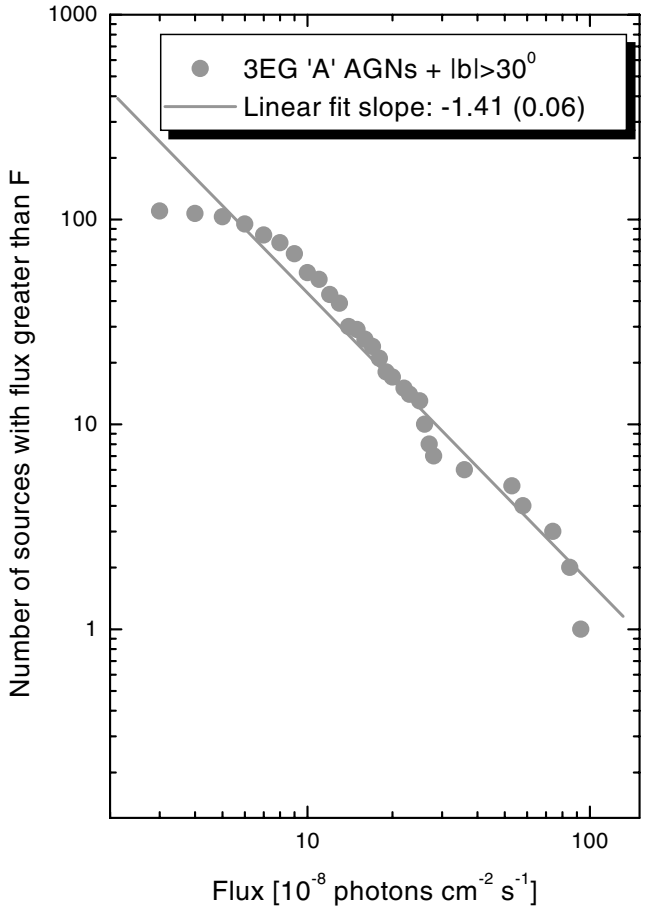

Figure 6. Log N–log F for the combined samples. The value of the linear fit slope (and error within parentheses) is shown. This figure can be seen in colour in the online version of the journal on *Synergy*.

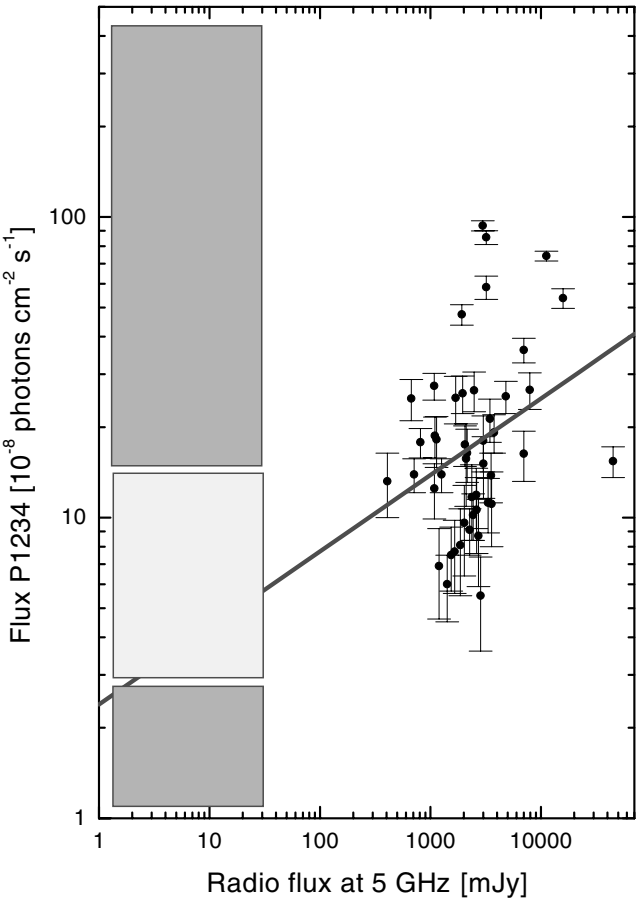

Figure 7. Radio and γ-ray fluxes of the 46 most likely AGN detections. The big vertical box signals the threshold sensitivity in the radio surveys used to search for counterparts (∼30 mJy). The middle box signals the range of γ-ray fluxes for the unidentified sources considered in these paper. This figure can be seen in colour in the online version of the journal on *Synergy*.

It is usually thought to be produced in a relativistic jet through inverse Compton scattering of lower-energy photons (e.g. Blandford & Levinson 1995). The soft, seed photons for the inverse Compton process could originate as synchrotron emission from within the jet, or they could come from the accretion disc surrounding the central supermassive compact object, or they could be disc radiation reprocessed in the broad line region. In the last two cases the seed photons are external to the jet itself.

In addition to these leptonic models, some hadronic alternatives have been proposed in the literature. The γ-ray emission would be produced in this case by relativistic protons interacting with ambient matter, radiation fields, or the magnetic field of the jet. For reviews and references the reader can see von Montigny et al. (1995) and Mukherjee (2001).

Independently of how the γ-rays are produced, they must traverse the strong X-ray field produced in the innermost region of the accretion disc. The observed γ-ray photons cannot originate from a too small radius, otherwise they will be absorbed through pair creation in the disc photosphere (e.g. Becker & Kafatos 1995; Blandford & Levinson 1995). This naturally leads to the concept of γ-spheres in AGN: for each γ-ray photon energy there is a radius r_γ beyond which the pair production opacity to infinity equals unity (Blandford & Levinson 1995). The size of the γ-sphere will depend on both the energy of the γ-ray photons and the soft photon flux.

For an isotropic, power-law, central source of soft photons scattered by free electrons in a warped disc, Blandford & Levinson (1995) obtain

$$r_\gamma(E) \propto E^p, \tag{6}$$

with p depending on the details of the central source. A similar result is obtained for pure disc emission (Becker & Kafatos 1995; Romero et al. 2000). Typically, $p \in [1, 2]$. The larger γ-spheres, then, are those for the higher photon energies. This energy dependence of the source size will naturally lead to chromaticity effects during microlensing events.

4 MICROLENSING

The characteristic time of a microlensing event is the time that the source takes to cross the Einstein radius of the lens. It is given by

$$t_0 = \frac{R_{\rm E}}{v} = \left(\sqrt{\frac{4GM}{c^2}\frac{D_{ol}D_{ls}}{D_{os}}}\right) v^{-1}, \tag{7}$$

where v is the lens velocity. For a cosmological source, t_0 is obtained using a cosmological model of the Universe, such that the angular diameter distances can be computed. Typical time-scales, for usual values of redshifts ($z_{\rm source} \sim 1$; $z_{\rm lens} \sim 0.1$–0.5) and typical stellar masses and velocities are in the range of hundreds of days.

The width of the peaks in the light curves (see equation 11 below) is approximately $\Delta t \simeq 0.05\, t_0$. It is interesting to compare such numbers with typical time-scales of high-latitude sources determined through the EGRET experiment. The third EGRET catalogue was constructed over a period of 6 years, dividing the total time-span into viewing periods with a duration of approximately 15 d. When the mass of the lensing object is subsolar, each peak in a microlensing light curve can be completely within a single EGRET viewing period: the phenomenon can lead, in principle, to a very variable source, with γ-ray fluxes varying from detection to upper limits in consecutive viewing periods. In contrast, for a 5-$M_\odot$ star, a single peak would last several viewing periods and the γ-ray source could appear as a steady, non-variable detection.

We have mentioned before that in order for a usual microlensing event to occur, the linear size of the source, x, should be less than the Einstein radius, $x \langle 2R_E(D_{os}/D_{ol})$. For a source with $x = 10^{14}$-cm strong magnification would typically occur for objects with masses $M/M_\odot \geqslant 2 \times 10^{-3}$. This makes most of the massive compact halo- (MACHO-) like objects in a galaxy able to produce strong gravitational lensing effects upon the innermost regions of background active galactic nuclei. The smaller masses can give rise to very rapid events (Romero et al. 1995).

The concept of optical depth, Γ, was originally introduced in gravitational microlensing studies by Ostriker & Vietri (1985), and it was later applied by Paczyński (1986). If Γ is smaller than unity, it provides a measure of the probability of microlensing. Alternatively, Γ can be defined as the ratio of the surface mass density of microlensing matter to the critical mass density of the galaxy (Paczyński 1986). The value of Γ depends on the model adopted for the matter distribution along the line of sight.

It is usually assumed that the a priori probability of finding a small group of distant, gravitationally magnified objects is below 1 per cent. Recent results (Wyithe & Turner 2002), taking into account the clustering of stars in interposed galaxies, give values of between 10^{-2} and 10^{-3} for the a priori probability of finding magnified sources in random directions of the sky. In those directions where there is gravitational lensing, the probability of having large local values of optical depth is high.

The high surface mass density associated with the core of normal galaxies along with the usual assumption that most of this mass

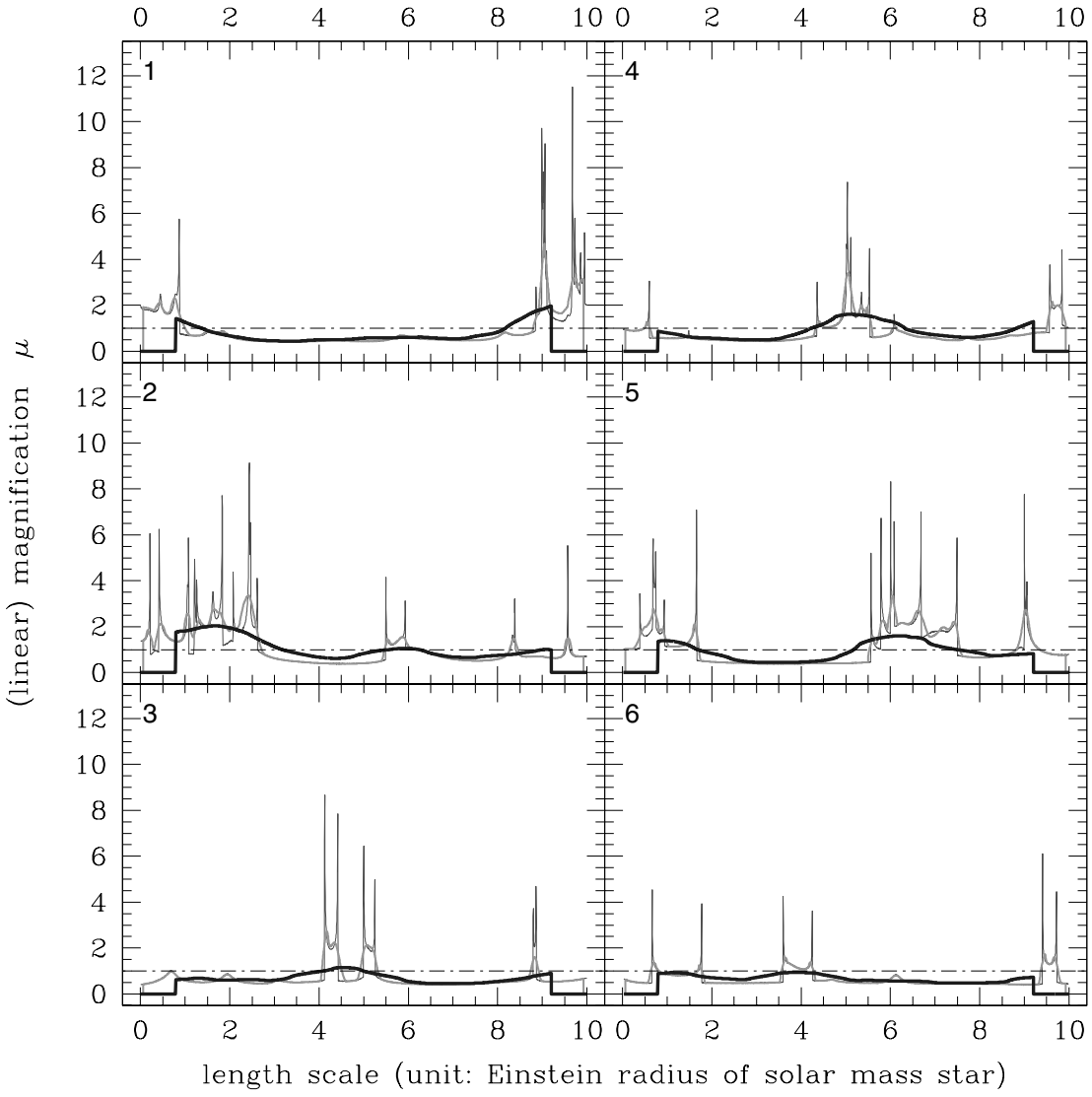

Figure 9. Light curves for different source trajectories. Numbers corresponds to those given in Fig. 8. Darker lines corresponds, respectively, to regions emitting photons of 100 MeV, 1 and 10 GeV, and with the emitting sizes depicted in the bottom left corner of Fig. 8, being the innermost point the less energetic γ-ray sphere. This figure can be seen in colour in the online version of the journal on *Synergy*.

is in the form of compact objects naturally leads to high optical depths for microlensing. For instance, in the case of the lensed quasar Q2237+0305, where four images are well-resolved, lensing models indicate values of $\tau \sim 0.5$ (Schneider et al. 1988; Wambsganss & Paczyński 1994), which are corroborated by the detections of microlensing-based optical variability with relatively high duty cycles (e.g. Corrigan et al. 1991; Witt & Mao 1994; Wozniak et al. 2000). Other lensed sources display even higher duty cycles (e.g. Koopmans & de Bruyn 2000).

In our case, the number of potential compact γ-ray-emitting background sources is large. The latest version of the Véron-Cetty & Véron (2001) catalogue – which is still very incomplete at high redshifts – contains more than 10^3 already identified blazars, in addition to more than 10^4 quasars and other less energetic AGN. The GLAST mission itself is expected to pinpoint approximately 10^4 γ-ray-emitting blazars with unparalleled resolution (Gehrels & Michelson 1999); also the number of unidentified sources at high latitudes is expected to be large. If the actual total number of γ-ray-emitting blazars is in excess of, say, 10^7 (one blazar out of 10 000 normal galaxies), they could produce many of the expected detections by GLAST. Even when considering reduced probabilities for microlensing, scaling as τ/A^2 with τ being the local optical depth and A the magnification, an interesting number of detections could be potentially ascribed to microlensing.

A crude estimation of the number of possible γ-ray sources produced by microlensing can be obtained as the product of three factors: random lensing probability × local lensing probability × number of background sources, i.e. approximately $\times 10^{-3} \times 1/A^2 \times 10^7$. The uncertainty in the previous expression, however, is large. We can only roughly estimate the total number of background sources, but the value of A they need to become visible, i.e. with fluxes above the sensitivity of EGRET and/or GLAST, will depend on the luminosity function of γ-ray-emitting AGN, which is unknown. According to the different sensitivities of both instruments, we could expect, perhaps, a number of detections of ∼10 and ∼100, respectively.

5 MAGNIFICATION MAPS

The parameters that describe a microlensing scenario are the dimensionless surface mass density κ – expressed in units of the critical

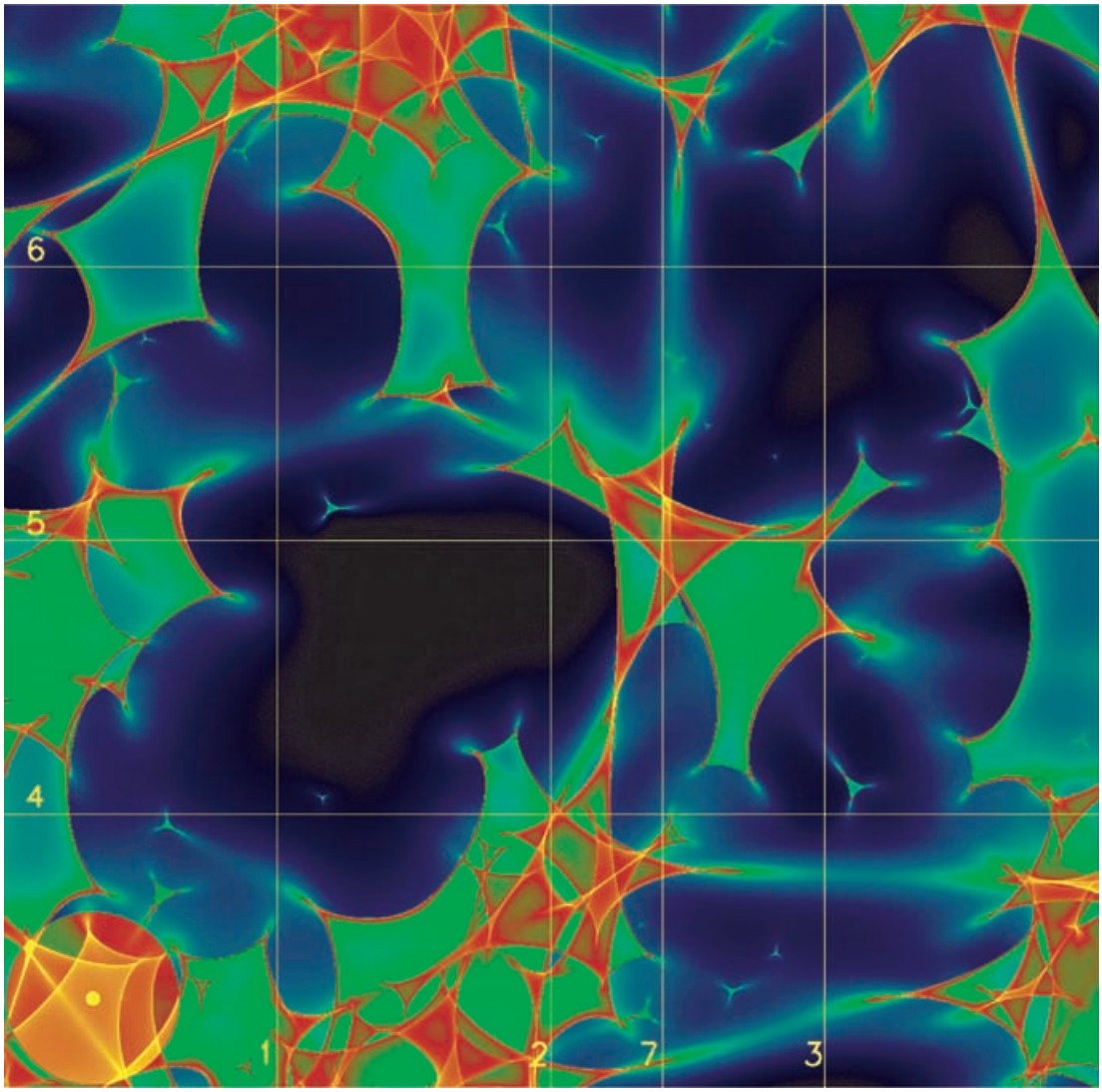

Figure 8. Magnification map for lensing with parameters $\kappa = 0.5$ and $\gamma = 0.0$ (for details see the text).

surface mass density – and the external shear γ (cf. Kayser, Refsdal & Stabell 1986; Schneider & Weiss 1987). The former – often also called convergence or optical depth – describes the amount of matter in front of the source. The latter is a tidal force caused by matter outside the light bundle. In order to simulate the effect of a particular combination of κ and γ, point lenses are distributed randomly according to the given surface mass density. If we were to replace each point lens by a disc with radius equal to its Einstein radius, the total fraction of the sky that is covered by the sum of all these discs is equal to the optical depth.

For the ray-shooting simulations, a large number of light rays (of the order of 10^9) are followed *backwards* from the observer through the field of point lenses. The number of rays determine the resolution of the numerical simulation. These rays start out in a regular (angular) grid. In the lens plane, the deflections according to the individual lenses are then superposed for each individual ray i,

$$\bar{\alpha}_i = \sum_{j=1}^{n} \bar{\alpha}_{ij} = \frac{4G}{c^2} \sum_{j=1}^{n} M_j \frac{\bar{r}_{ij}}{r_{ij}^2}, \tag{8}$$

where M_j is the mass of the point lens j, $\bar{r}_{ij}$ is the projected vector distance between the position of the light ray i and the lens j, and r_{ij} is its absolute value. It is the computations of these individual deflections that requires most of the computation time for the simulation. The effect of the external shear is included as well. The deflected rays are then followed further to the source plane. There, they are collected in small pixels. The number of rays per pixel (on average $\sim$100 for a region typically of 2500 $\times$ 2500 pixels) is proportional to the magnification at this position. A two-dimensional map of the ray density – a magnification pattern, also referred to as a caustic pattern – can then be produced. The magnification as a function of (source) position is indicated by colours. Sharp lines correspond to locations of very high magnification, i.e. the caustics. A detailed account of the numerical technique can be found in Wambsganss (1999).

In general, a smoothed out distributed surface mass density κ_c also contributes to the deflection as well, and the general microlensing equation to be solved is

$$y = \begin{pmatrix} 1-\kappa-\gamma & 0 \\ 0 & 1-\kappa+\gamma \end{pmatrix} \bar{x} - \kappa_c \bar{x}. \tag{9}$$

In observational situations $\kappa_{tot} = \kappa + \kappa_c$ and γ are obtained from macrolensing simulations of the resolved source. Rays representing a square are then mapped on to a rectangle with a side ratio $T =$

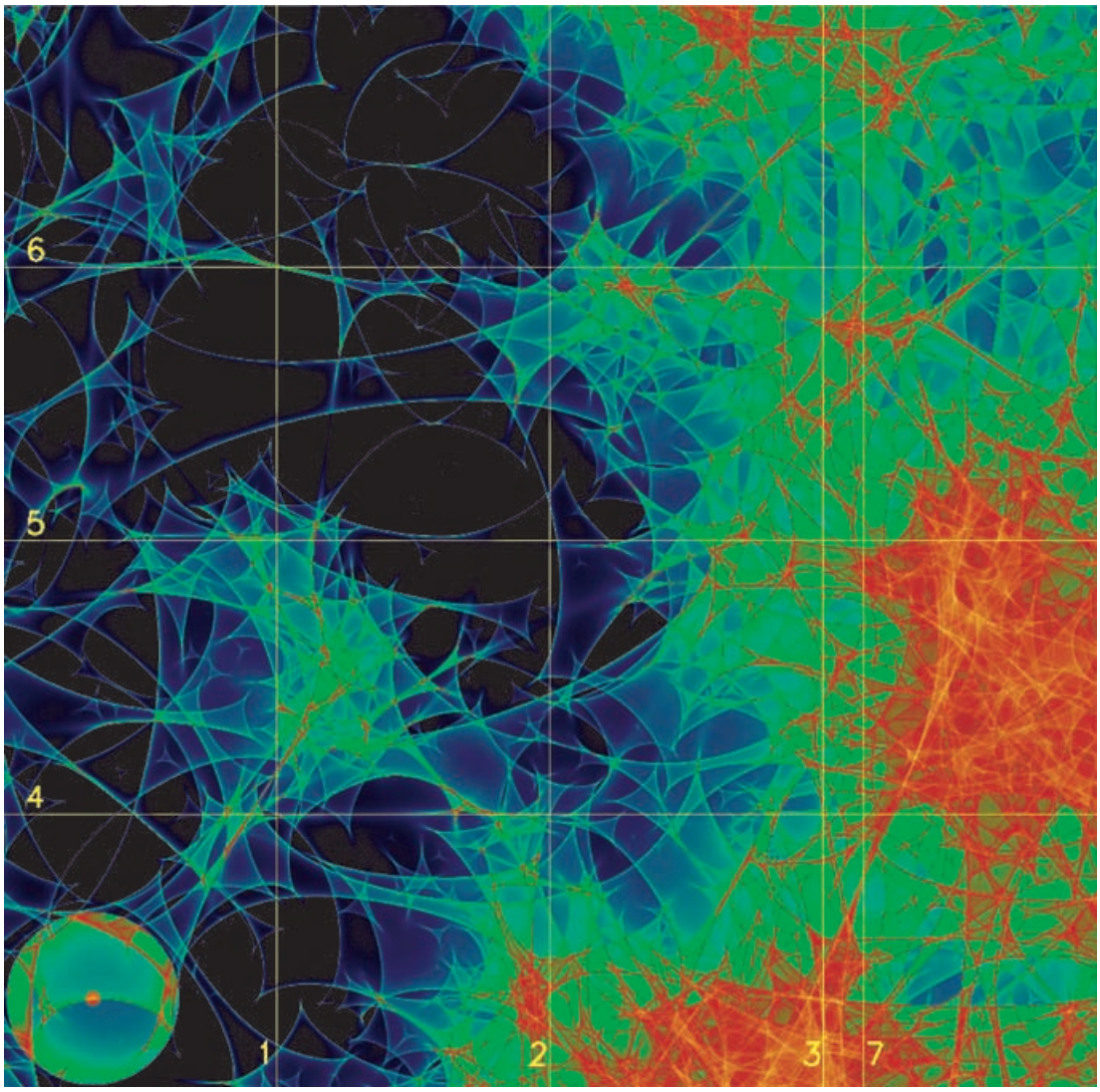

Figure 10. Magnification map for lensing with parameters $\kappa = 0.8$ and $\gamma = 0.0$ (for details see the text).

$(1-\kappa-\kappa_c-\gamma)/(1-\kappa-\kappa_c+\gamma)$. However, as we would like the receiving – and not the shooting – area to be a square (the pixel) the shooting field (i.e. the area in the lens plane in which rays are mapped) is chosen to be a rectangle of size T^{-1}.

Fig. 8 shows the magnification map for the case in which $\kappa = 0.5$ and $\gamma = 0.0$; the brighter the region, the stronger the magnification. The characteristic critical lines of the Chang–Refsdal (1984) model appear in this map, and the diamond-shaped structures owing to the close-by star. In the bottom left of the panel, we show the size of the source for three different energies. The innermost pixel (the centre of the circles) represent the size of the lowest-energy γ-sphere, which corresponds to $E = 100$ MeV. The second circle is the size of the 1-GeV γ-sphere, whereas the largest one is the corresponding size of the $E = 10$ GeV emitting region. The origin of the differential magnification is obvious: the γ-spheres will be affected according to their size while moving in the caustic pattern.

The numbered lines in Fig. 8 represent different source trajectories. Numbers 1–6 are trajectories common to all maps we shall present, and these positions are defined a priori. The light curves for each of these six trajectories are given in Fig. 9. In a lighter colour we show, for each trajectory, the corresponding light curve for the $E = 100$ MeV emitting region. Darker lines correspond to regions emitting photons of 1 and 10 GeV. The latter, in all cases, are smoother versions of the former and, always, the magnification fluctuations are weaker for these regions. There is a typical factor of 10 more magnification for the innermost regions than for the larger γ-spheres. We see that for these values of κ and γ it is possible to obtain a typical enhancement of 10 times the unlensed intensity at 100 MeV. (The drop to zero at the corners of the diagram for all light curves corresponding to the largest γ-sphere is an artefact of the simulations: the code assigns zero magnification when more than half of the source is out of the magnification map.)

The shape of the light curves is also worth a comment. As an example, we take trajectory 3 of Fig. 8. It starts in a region of low magnification and continues upwards, crossing a region of relatively high enhancement, where for the innermost γ-sphere the magnification is nine times the intensity of the unlensed source. There are four caustic crossings there. We can see that for the innermost γ-sphere, the caustic crossings are well-separated events, so we have four peaks in the light curve corresponding to $E = 100$ MeV. However,

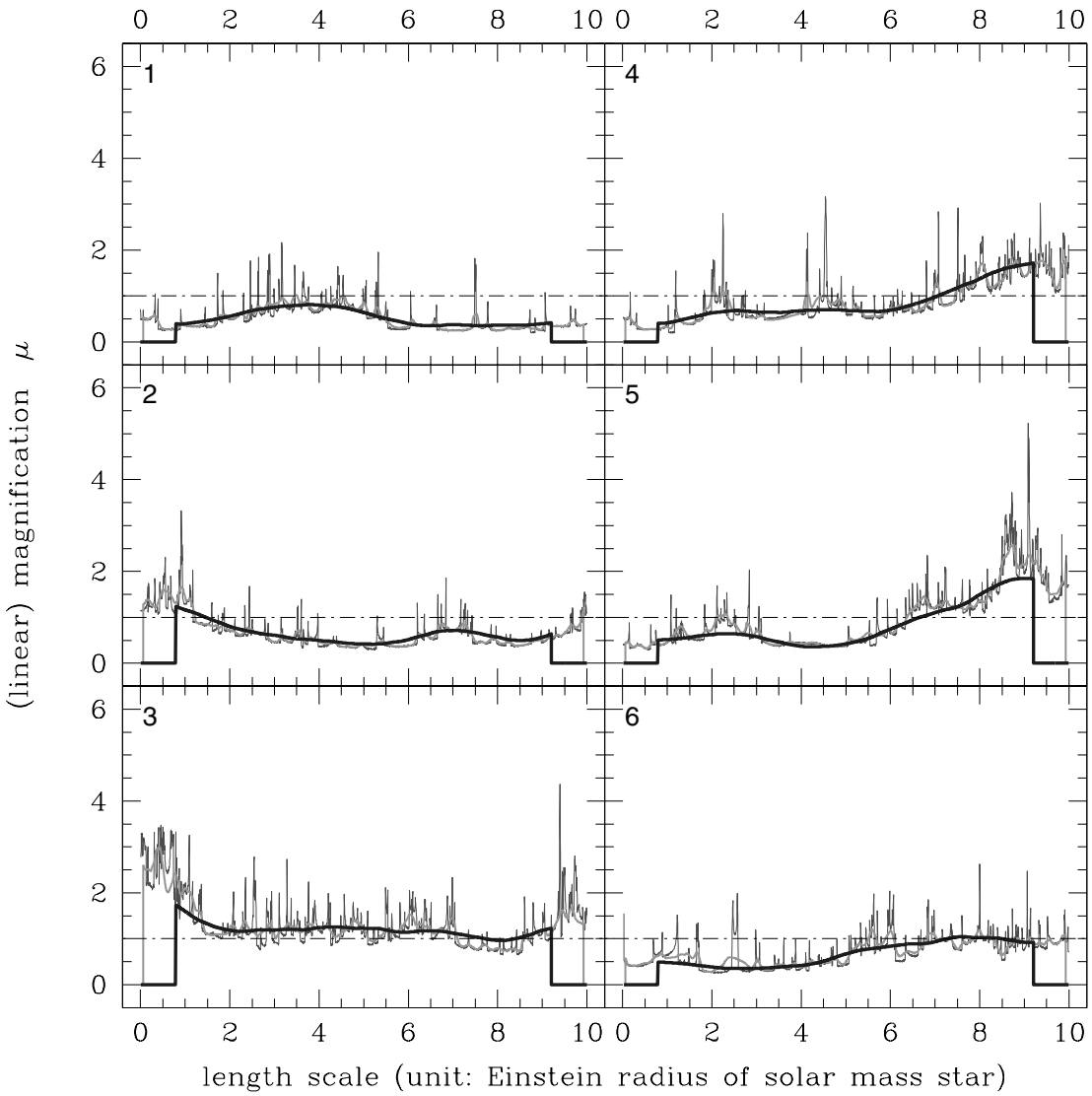

Figure 11. Light curves for different source trajectories. Numbers corresponds to those given in Fig. 10. The line coding is as in Fig. 9. This figure can be seen in colour in the online version of the journal on *Synergy*.

for the larger γ-spheres the peaks are smoothed down. We see only two broadened peaks for $E = 1$ GeV, and only one, with almost nil magnification, in the case of $E = 10$ GeV. If the γ-ray AGN is within the observing sensitivity, we would see a distinctive effect during the microlensing event owing to the different sizes of the source at the different energies.

The x-axis in Fig. 9 is a linear length-scale, the Einstein radius of a solar mass star, $R_E(\mathrm{M}_\odot) = 2.23 \times 10^{16}$ cm. It can be translated into a time-scale as $t = R_E(\mathrm{M}_\odot)/v$, where v is the relative velocity of the source with respect to the lens, projected on to the source plane. To give an example of the time-scales predicted with a full caustic pattern plot, we write the time-scale as

$$t = \frac{R_E(\mathrm{M}_\odot)}{v} = \frac{0.023}{v/c}\mathrm{yr}. \tag{10}$$

With a relative velocity, i.e. the combination of all velocities projected on to the source plane, $v = 5000$ km s^{-1}, the length of each axis in Fig. 8 is equivalent to 14 yr. The other important time-scale involved in a microlensing event is the rise time to a peak of maximum magnification. This will depend on the size of the different γ-spheres, and is given by

$$\tau = \frac{R}{v} = \frac{0.023}{v/c}\frac{R}{R_E(\mathrm{M}_\odot)}\mathrm{yr}, \tag{11}$$

where, again, we have scaled it with the Einstein radius corresponding to one solar mass. Then, the innermost γ-spheres (having $R/R_E \sim 1/100$) will have a rise time-scale of approximately 5 d, well within an observing EGRET viewing period. The largest γ-spheres, with $R \sim R_E$, can have a rise time of approximately 1 yr. Higher (lower) velocities would imply lower (higher) time-scales.

Fig. 10 shows the magnification map corresponding to a higher value of focusing, $\kappa = 0.8$ and $\gamma = 0$. As was found by Schneider & Weiss (1987), the critical structure become more complex with increasing κ and it is no longer possible to identify a constellation of compact objects. In addition, we also see (as in Fig. 8) the tendency of the caustic structure to cluster, generating some crowded critical regions and some others devoid of high magnification patterns. The explanation for this was already given by Schneider & Weiss (1987): the clustering of caustics is just the non-linear enhancement of random (Poisson) clustering of the positions of lenses in the source plane.

The magnitude of the magnification has been typically reduced with respect to the $\kappa = 0.5$ case: see Fig. 11. The density of caustics

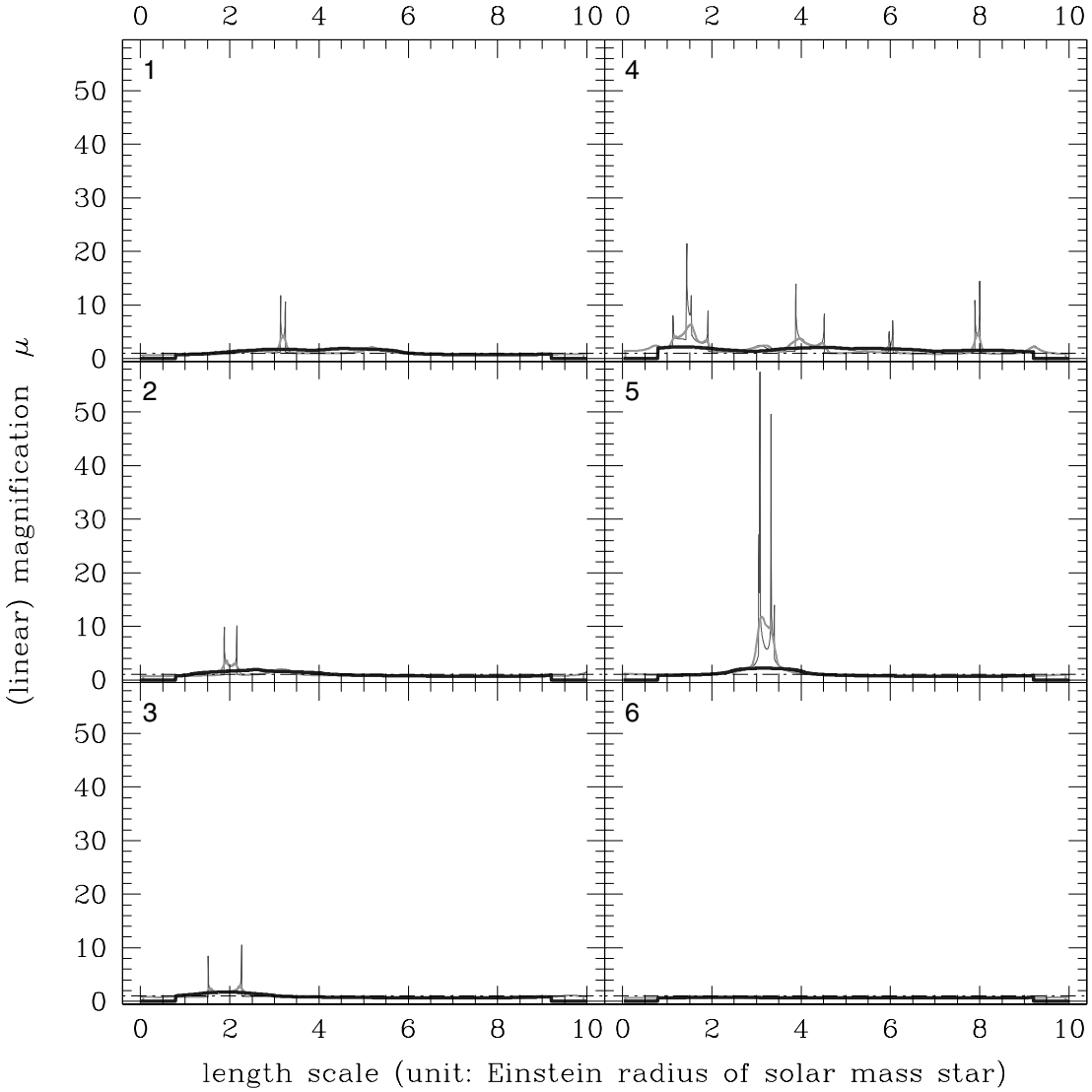

Figure 13. Light curves for different source trajectories. Numbers corresponds to those given in Fig. 12. The line coding is as in Fig. 9. This figure can be seen in colour in the online version of the journal on *Synergy*.

is so large that the light curve is continuously affected by them, producing a less dramatic combined effect. This effect was first studied by Deguchi & Watson (1987): the total magnification is always high, but the fluctuations decreases beyond $\kappa = 0.5$. Again, the differential effect is notorious.

Fig. 12 shows the magnification pattern for the case $\kappa = 0.2$ and $\gamma = 0.16$. The presence of shear modifies qualitatively the magnification map. Here, most of the map is devoid of magnification, and so, many of the common trajectories (numbers 1–6) cross large regions of very low or nil magnification (see particularly trajectory 6). However, those trajectories actually crossing the caustics produce enhancements in intensity typically between 10 and 20 times the unlensed value. These effects can be seen in the six panels of Fig. 13. In addition, the enhancements of intensity are usually well separated (see, for instance, trajectory 4). From the point of view of unidentified γ-ray sources, interposed galaxies with low values of κ and γ are probably the most interesting case for the application of the model.

Finally, in Fig. 14 we show the magnification map corresponding to the case $\kappa = 0.9$ and $\gamma = 0.4$. Again, the high value of κ makes the critical structure highly complex. Typically, the magnification values are below a factor of 10 of the unlensed intensity, although some trajectories are found (see, for example, curves number 3 and 4 of Fig. 15) where a factor of $\sim$10 is reached in two well-separated regions.

In order to explore the maximum possible magnification that these caustic patterns produce, we have selected an extra trajectory for each map that crosses exactly over a conjunction of several caustics (trajectory 7 in all maps). The light curve for these cases is shown separately in Fig. 16. We can see that magnifications up to 65 times the unlensed intensity of the source are possible for the examples shown. The probability for these trajectories actually occurring is much less than fluctuations with average amplitude. However, even if the probability is reduced by, say, a factor $1/A^2$, it is possible to expect many cases of high magnification.

6 SUMMARY AND FINAL COMMENTS

To summarize, we have shown in this paper that:

(i) some of the high-latitude unidentified γ-ray sources (both variable and non-variable) could be weak γ-ray-emitting AGN that

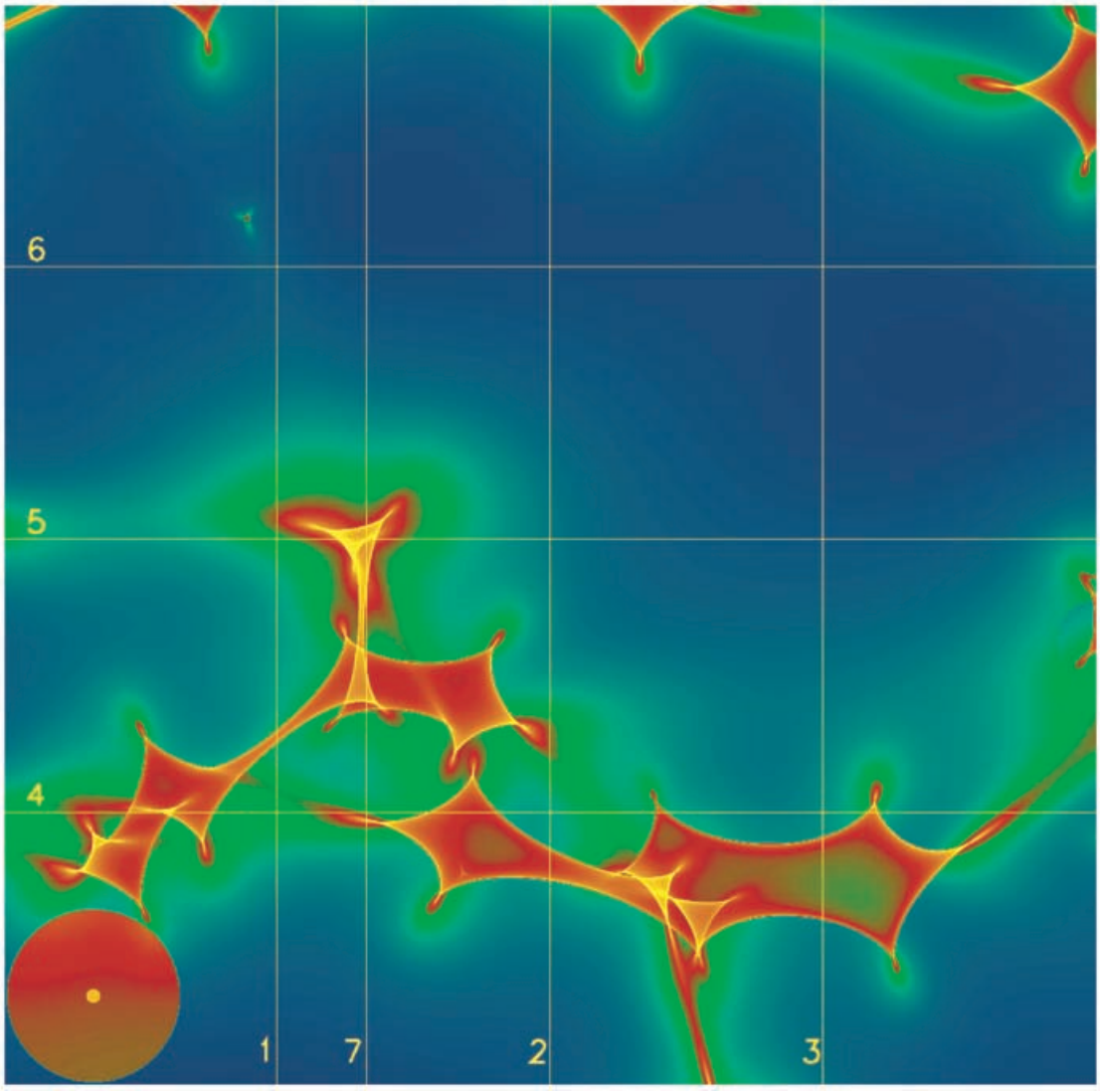

Figure 12. Magnification map for lensing with parameters $\kappa = 0.2$ and $\gamma = 0.16$ (for details see the text).

are magnified through gravitational microlensing by stars in foreground galaxies;

(ii) although small, the probability of gravitational microlensing could be enough to explain a handful of the EGRET detections, and possibly many of the forthcoming GLAST detections;

(iii) the differential magnification makes its way to a spectral slope change at medium energies (During a γ-ray variability event produced by microlensing of a blazar, there is a peculiar spectral evolution that could be detected, in principle, by the next generation of γ-ray observatories with fine spectral capabilities, such as GLAST, or even by ground γ-ray telescopes located at sufficient altitude, such as 5@5, e.g. Aharonian et al. 2001).

It should be clearly stated that this model cannot account for all unidentified γ-ray detections at high latitudes. However, it is interesting to ask whether the proposed microlensing scenario could be responsible for γ-ray variability of some radio-loud AGN already detected by EGRET. Indeed, there is one possible case, related with the source 3EG J1832–2110, which has been identified with PKS 1830–211 (Mattox et al. 1997; Combi & Romero 1998). The latter is a flat-spectrum radio source, proposed to be a gravitational lensed quasi-stellar object (QSO) by Pramesh Rao & Subrahmanyan (1988). The γ-ray source is probably variable, presenting a value of $I = 2.5$, and a steep spectral index, $\Gamma = 2.59 \pm 0.13$. Both facts, variability and a steep spectra, argue against a galactic origin for this source. Mattox et al. (2001) assign to this pair an a priori probability of 0.998 of being correct, and list it within the most likely AGN identification of the third EGRET catalogue.

High-resolution radio images obtained from several interferometric arrays have revealed that the source has a ring-like structure with two bright components on subarcsecond scales (Jauncey et al. 1991). This suggests a close alignment of the lensed source behind the lensing object. Two absorption systems have been detected at $z \sim 0.89$ (Wiklind & Combes 1996) and $z \sim 0.193$ (Lovell et al. 1996), so it seems likely that the image of the background QSO (with a redshift $z > 0.885$, Mattox et al. 2001) is lensed by two different extragalactic objects, what would undoubtedly enhance the optical depth and the number of expected single microlensing events.

Indeed, Combi & Romero (1998) have already proposed that the γ-ray emission of 3EG J1832–2110 (then 2EG J1834–2138) could be produced by gravitational microlensing, using exactly the same ideas we have explored in this paper. They have found that assuming

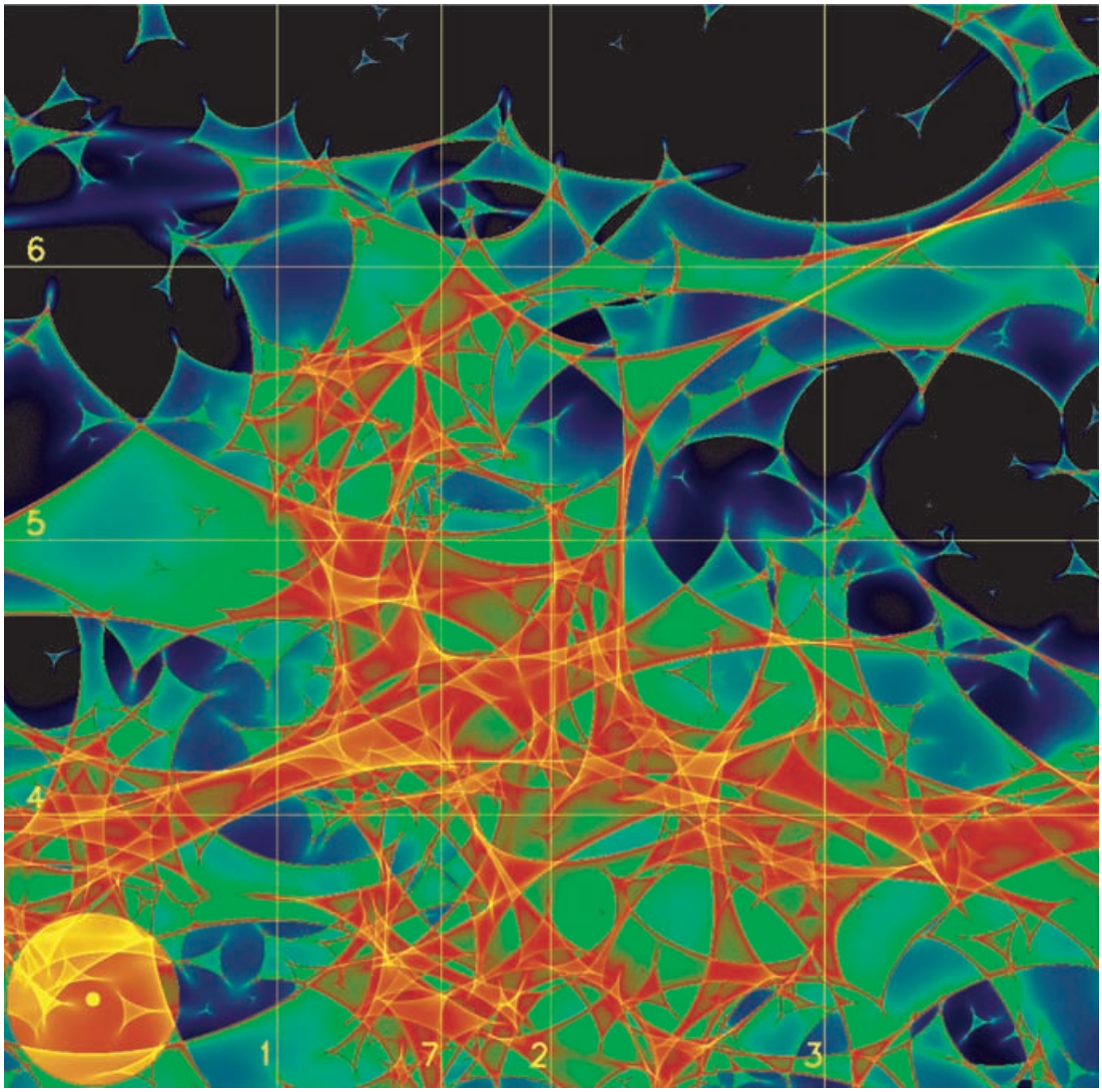

Figure 14. Magnification map for lensing with parameters $\kappa = 0.9$ and $\gamma = 0.4$ (for details see the text).

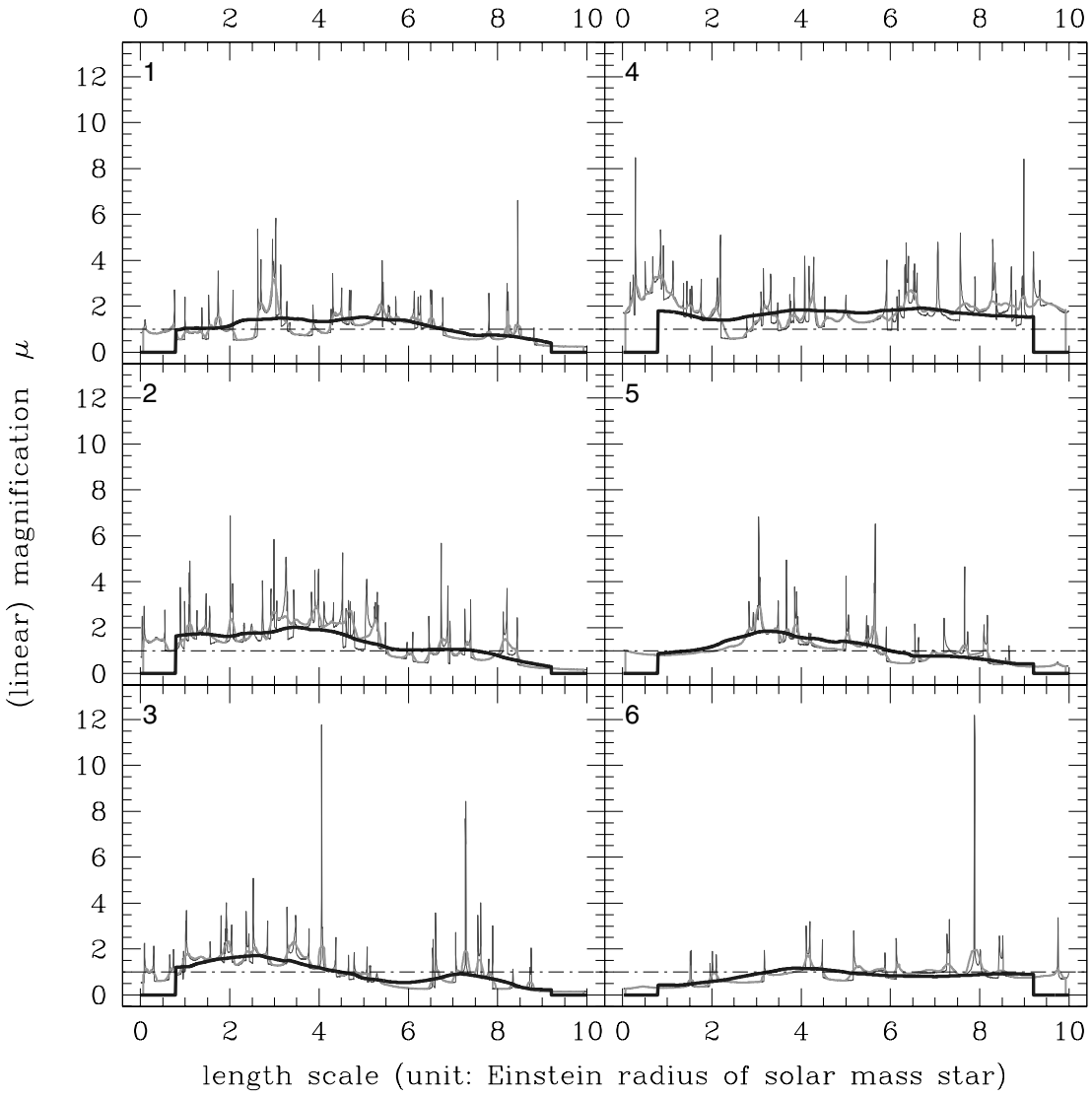

Figure 15. Light curves for different source trajectories. Numbers corresponds to those given in Fig. 14. The line coding is as in Fig. 9. This figure can be seen in colour in the online version of the journal on *Synergy*.

a redshift $z_s = 1$ for the background source and $z_l \sim 0.89$ for the lens, a MACHO-like object with $M \sim 0.02\,M_\odot$ and moving with a low velocity of only $v \sim 1000$ km s^{-1} would be enough to produce the observed variability. For this to be possible, the size of the γ-ray-emitting region should be of approximately 1.5×10^{15} cm, in good agreement with the source sizes used in this paper. These results can be slightly modified by new measurements of the quasar redshift, but will not change substantially (Oshima et al. 2001).

It is likely then that the first realization of this proposed mechanism has been already observed for the pair 3EG J1832–2110/PKS 1830–211. One thing should be remarked, though: in this case the background source is already a strong radio emitter – which indeed facilitates the identification. This was not the general case we have considered here, where the sources are weak enough to yield no significant lower-energy counterparts.

Finally, let us assume that a correct alignment of source, lens and observer has been produced and that microlensing is operating. A possible astrophysical application of the effects we have discussed in the previous sections is to constrain the exponent in the relationship between size and energy for γ-ray spheres in the AGN, $R \propto E^\alpha$. The smaller the source, the higher is the peak γ-ray luminosity, and the shorter the resulting rise time-scale ($\tau = R/v$). Therefore, by observing throughout the peak at different energies, one could determine the relative size of the source at such energies, and then test the radius–energy theoretical relationship. This could be done within the range of GLAST capabilities. If, somehow, we know the relative velocity and the redshifts, we could even determine the sizes of the different emitting regions. This would directly impact on the underlying γ-ray models (e.g. Becker & Kafatos 1995; Blandford & Levinson 1995).

ACKNOWLEDGMENTS

This work has been supported by Universidad de Buenos Aires (UBACYT X-143, EFE), CONICET (PIP 0430/98, GER), ANPCT (PICT 98 no 03–04881, GER) and Fundación Antorchas (through separates research grants to GER and DFT). GER was on leave from IAR during part of this research. Also, part of his work was

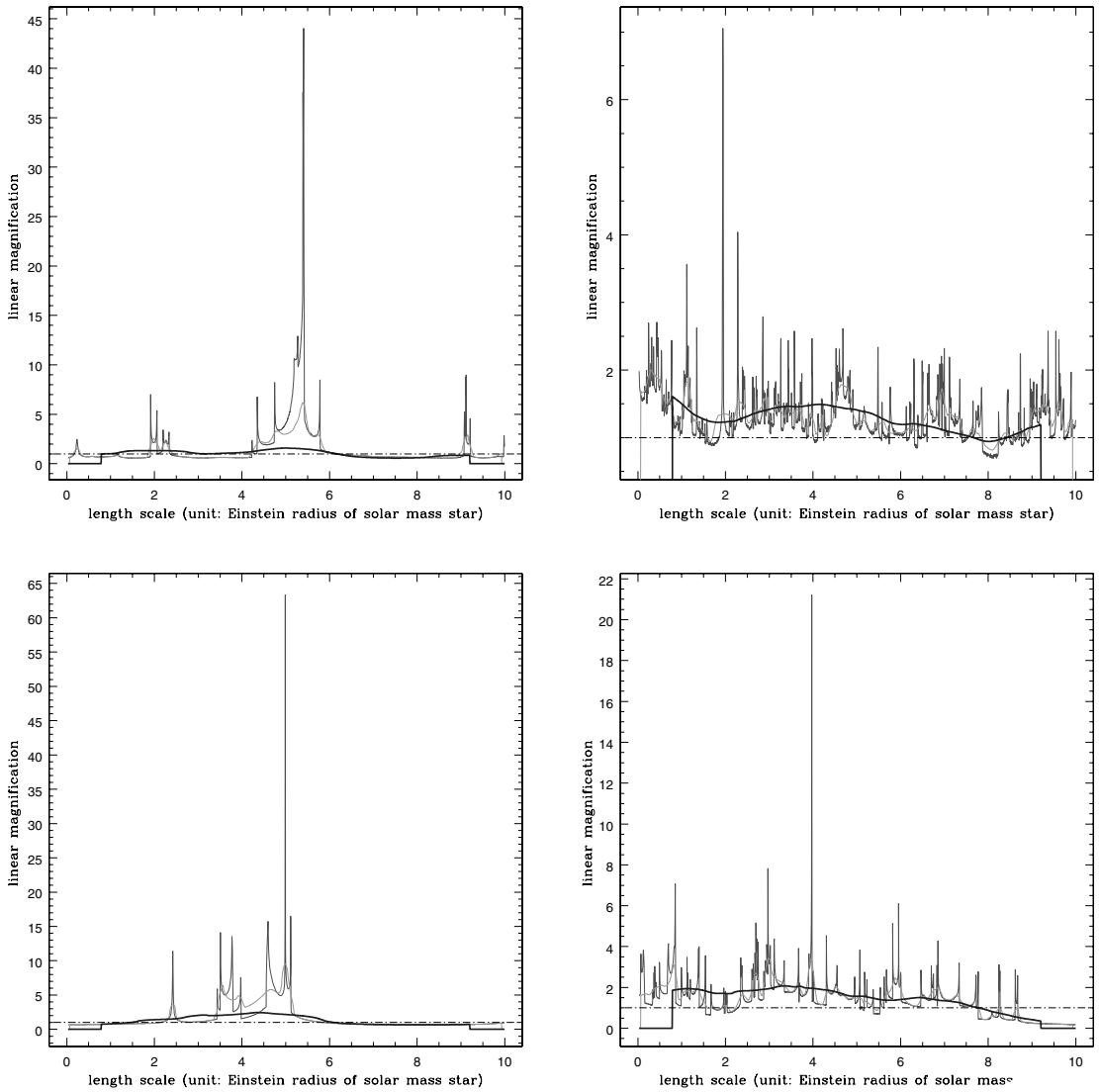

Figure 16. Light curve for trajectories labelled no 7, producing one of the highest levels of magnification out of the map given (from left to right and top to bottom) in Figs 8, 10, 9 and 14. The line coding is as in Fig. 9. This figure can be seen in colour in the online version of the journal on *Synergy*.

also performed under the auspices of the US Department of Energy by University of California Lawrence Livermore National Laboratory under contract no W-7405-Eng-48. DFT is LLNL's Lawrence Fellowship in Astrophysics. We acknowledge insightful comments by Drs E. Turner, R. Hartman and D. Thompson in an early stage of this research, and critical remarks from an anonymous referee who contributed to improving the paper.

REFERENCES

Aharonian F.A., Konopelko A.K., Völk H.J., Quintana H., 2001, AP, 15, 335
Benaglia P., Romero G.E., Stevens I., Torres D.F., 2001, A&A, 366, 605
Becker P., Kafatos M., 1995, ApJ, 453, 83
Blandford R.D., Levinson A., 1995, ApJ, 441, 79
Butt Y.M., Torres D.F., Combi J.A., Dame T., Romero G.E., 2001, ApJ, 561, L203
Camilo F. et al., 2001, ApJ, 557, L51
Chang K., Refsdal S., 1984, A&A, 132, 168
Combi J.A., Romero G.E., 1995, A&A, 303, 873
Combi J.A., Romero G.E., 1998, A&AS, 128, 423
Combi J.A., Romero G.E., Benaglia P., 1998, A&A, 333, L91
Combi J.A., Romero G.E., Benaglia P., Jonas J., 2001, A&A, 366, 1047
Corrigan R.T. et al., 1991, AJ, 102, 34
D'Amico N. et al., 2001, ApJ, 552, L45
Deguchi S., Watson W.D., 1987, Phys. Rev. Lett., 59, 2814
Esposito J.A., Hunter S.D., Kanbach G., Sreekumar P., 1996, ApJ, 461, 820
Garnavich P.M., Loeb A., Stanek K.Z., 2000, ApJ, 544, L11
Gehrels N., Michelson P., 1999, AP, 11, 277
Gehrels N., Macomb D.J., Bertsch D.L., Thompson D.J., Hartman R.C., 2000, Nat, 404, 363
Grenier I., 2000, A&A, 364, L93
Hartman R.C. et al., 1999, ApJS, 123, 79
Jauncey D.L. et al., 1991, Nat, 352, 132
Kaspi V.M., Lackey J.R., Mattox J., Manchester R.N., Bailes M., Pace R., 2000, ApJ, 528, 445
Kayser R., Refsdal S., Stabell R., 1986, A&A, 166, 36
Kaufman Bernadó M.M., Romero G.E., Mirabel I.F., 2002, A&A, 385, L10
Koopmans L.V.E., de Bruyn A.G., 2000, A&A, 358, 793
Koopmans L.V.E., Wambsganss J., 2001, MNRAS, 325, 1317
Lovell J.E.J. et al., 1996, ApJ, 472, L5
Mao S., Loeb A., 2001, ApJ, 547, L97

Mattox J.R., Schachter J., Molnar L., Hartman R.C., Patnaik A.R., 1997, ApJ, 481, 95
Mattox J.R., Hartman R.C., Reimer O., 2001, ApJS, 135, 155
Mukherjee R., 2001, in Aharonian F.A., Völk H.J., eds, High Energy Gamma-Ray Astronomy. AIP, Melville, p. 324
Oshima T., Mitsuda K., Ota N., Yonehara A., Hattori M., Mihara T., Sekimoto Y., 2001, ApJ, 551, 929
Ostriker J., Vietri M., 1985, Nat, 318, 446
Özel M.E., Thompson D.J., 1996, ApJ, 463, 105
Paczyński B., 1986, ApJ, 304, 1
Paczyński B., 1996, ARA&A, 34, 419
Paredes J.M., Marti J., Ribo M., Massi M., 2000, Sci, 288, 2340
Pramesh Rao A., Subrahmanyan R., 1988, MNRAS, 231, 229
Punsly B., 1998a, ApJ, 498, 640
Punsly B., 1998b, ApJ, 498, 660
Punsly B., Romero G.E., Torres D.F., Combi J.A., 2000, A&A, 364, 556
Reimer O., 2001, in Carramiana O., Reimer O., Thomson D., eds, The Nature of Galactic Unidentified Gamma-ray Sources. Kluwer, Dordrecht, p. 17
Reimer O., Thompson D.J., 2001, Proc. 27th Int. Cosmic Ray Conf. Copernicus Gessellschaft, Lindau, in press (astro-ph/0108348)
Romero G.E., 2001, in Carramiana O., Reimer O., Thomson D., eds, The Nature of Galactic Unidentified Gamma-ray Sources. Kluwer, Dordrecht, p. 65 (astro-ph/0012243)
Romero G.E., Combi J.A., Colomb F.R., 1994, A&A, 288, 731
Romero G.E., Surpi G., Vucetich H., 1995, A&A, 301, 641
Romero G.E., Benaglia P., Torres D.F., 1999, A&A, 348, 868
Romero G. E., Chajet L., Abraham Z., Fan J.H., 2000, A&A, 360, 57
Romero G.E., Kaufman Bernado M.M., Combi J.A., Torres D.F., 2001, A&A, 376, 599
Schlickeiser R., 1996, A&AS, 120, 481
Schneider P., Weiss A., 1987, A&A, 171, 49
Schneider D.P., Turner E.L., Gunn J.E., Hewitt J.N., Schmidt M., Lawrence C.R., 1988, AJ, 95, 1619
Sturner S.J., Dermer C.D., Mattox J.R., 1996, A&AS, 120, 445
Swanenburg B.N. et al., 1978, Nat, 275, 298
Thompson D.J., 2001, in Aharonian F.A., Völk H.J., eds, High Energy Gamma-Ray Astronomy. AIP, Melville, p. 103 (astro-ph/0101039)
Thompson D.J. et al., 1999, ApJ, 516, 297
Tompkins W., 1999, PhD thesis, Stanford Univ.
Torres D.F., Romero G.E., Combi J., Benaglia P., Andernach H., Punsly B., 2001a, A&A, 370, 468
Torres D.F., Combi J.A., Romero G.E., Benaglia P., 2001b, in Carramiana O., Reimer O., Thomson D., eds, Proc. Int. Workshop on the Nature of Galactic Unidentified Gamma-ray Sources. Kluwer, Dordrecht, p. 97 (astro-ph/0012160)
Torres D.F., Pessah M.E., Romero G.E., 2001c, Astron. Nachr. 322, 223
Torres D.F., Butt Y.M., Camilo F., 2001, ApJ, 569, 600
Torres D.F., Romero G.E., Eiroa E.F., 2002a, ApJ, 569, 600
Torres D.F., Romero G.E., Dame T., Combi J., Butt Y.M., 2002b, Phys. Rep., submitted (astro-ph/0209565)
Totani T., Kitayama T., 2000, ApJ, 545, 572
Véron-Cetty M.-P., Véron P., 2001, A&A, 374, 92
von Montigny C. et al., 1995, ApJ, 440, 525
Wambsganss J., 1999, J. Comp. Appl. Math., 109, 353
Wambsganss J., 2001, in Brainerd T., Kochanek C.S., eds, ASP Conf. Ser. Vol. 237, Gravitational Lensing: Recent Progress and Future Go. Astron. Soc. Pac., San Francisco, p. 185
Wambsganss J., Paczyński B., 1991, ApJ, 102, 864
Wambsganss J., Paczyński B., 1994, ApJ, 108, 1156
Wiklind T., Combes F., 1996, Nat, 379, 139
Williams L.L.R., Wijers R.A.M.J., 1997, MNRAS, 286, L11
Witt H.J., Mao S., 1994, ApJ, 429, 66
Wozniak P.R. et al., 2000, ApJ, 540, L65
Wyithe S., Turner E.L., 2002, ApJ, 567, 18
Zhang L., Zhang Y.J., Cheng K.S., 2000, A&A, 357, 957

This paper has been typeset from a TEX/LATEX file prepared by the author.